SISSA - SCUOLA INTERNAZIONALE SUPERIORE DI STUDI AVANZATI
TRIESTE
Strada Costiera 11

ISAS - INTERNATIONAL SCHOOL FOR ADVANCED STUDIES

Thesis submitted for the degree of
"Magister Philosophiae"

SHORT TERM X-RAY AGN VARIABILITY

CANDIDATE
Bao Gang

SUPERVISOR
Prof. Marek A. Abramowicz

Academic Year 1989/90

TRIESTE

Scuola Internazionale Superiore di Studi Avanzati

International School for Advanced Studies

SHORT TERM X-RAY AGN VARIABILITY

Thesis submitted for the degree of

"Magister Philosophiæ"

CANDIDATE

Bao Gang

SUPERVISOR

Prof. Marek A. Abramowicz

October 1990

Chapter 1

Introduction

PART 1

Since Active Galactic Nuclei was widely acknowledged as an important astrophysical phenomenon (Burbidge, et al. 1963, Robinson et al. 1964), 26 years have past. It is now generally believed that Active Galactic Nuclei are powered by gravitational potential energy as matter is accreted into a central massive black hole ($\sim 10^6 - 10^9 M_\odot$). The black hole and its surrounding accretion disk are responsible for phenomena ranging in lengthscales from giant radio sources ($\sim 10^{22} - 10^{25} cm$) through narrow emission line regions ($\sim 10^{20} - 10^{22}$ cm), compact radio sources ($\sim 10^{18} - 10^{21}$cm), broad emission line region ($\sim 10^{18} - 10^{19}$ cm), "thermal" bumps and non-thermal continua ($\sim 10^{15} - 10^{17}$ cm), down to the shortest scales associated with rapid X-ray variability ($\sim 10^{13}$ cm) (Blandford, 1985). The emitted photon energy ranges from lowest radio to highest γ- ray energies.

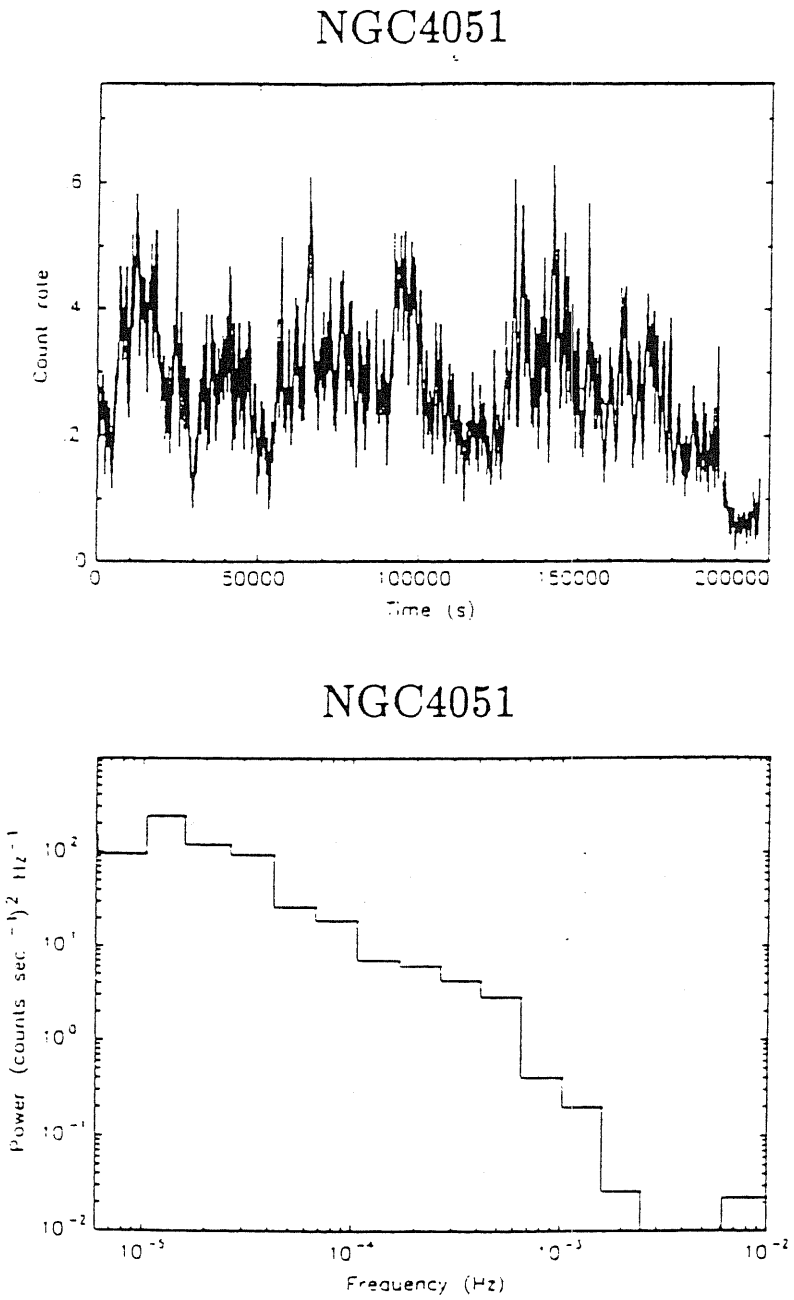

Figure 1. LE light curve and power spectrum for Active Galactic Nuclei NGC 4051(McHardy, 1989)

In this dissertation, we are interested in the X-ray emission region, the inner part of accretion disk. It is generally accepted that most of X-ray comes from $r_{in} < r < 10r_g$(Abramowicz et al, 1989), r_g is gravitational radius ($r_g = \frac{2MG}{c^2}$), r_{in} is the inner radius of accretion disk, which is somewhere between $3r_G$ for very slowly rotating black hole and $\sim 1/2r_G$ for rapid rotating one (extreme Kerr black hole).

Fig. 1 is the typical X-ray light curve and its power spectrum for Active Galactic Nuclei NGC 4051. We can see that the X-ray light curve shows rapid variability, which reflects interesting physical process of that region. Fig .1 suggests that the inner region of AGN is not "quiet".

In order to examine more closely the flux variation with time, one can calculate its corresponding power spectrum. The power spectrum refers to the strength of the signal at given frequency ω or at its corresponding time interval. From the observational point of view, the power spectrum is

$$p(\omega) = \left(\frac{counts}{sec}\right)^2 = (amplitude)^2 \tag{1.1}$$

and mathematically, it is square of the Fourier transform of the signal. (see below). The power spectrum method is a very important tool to investigate how fast the signal changes and particularly to search the characteristic timescales.

After over 20 years of accumulation of observational data from different satellites, especially from the "long looks" of EXOSAT, it is found that for X-ray photons in the energy range of 2-10kev the energy flux of most samples varies at all time scales. The variability shows no feature in most cases and its power spectrum appears in a power-law shape,

$P \sim \omega^{-\beta}$ in the frequency range of $10^{-5} - 10^{-3}$ Hz(Pounds et al 1988). The power-law index β is in the range of 1-2. The power spectra of high energy X-rays from the galactic black hole candidate Cyg X-1, neutron star binary and low mass X-ray binaries (LMXBs) also exhibit the same power-law behavior in their power spectra of their X-ray light curves in the frequency range of 0.1-10 Hz. These frequencies roughly scale with mass.

Power law behavior means that the physics of variability of AGN and in the observed range is self-similar, timescale-invariant, or short of characteristic timescale. The possible exception of this behavior is NGC 6814 in whose power spectrum several peaks were found.

To understand self-similar behavior clearly, let us consider the timescale-invariant power spectrum $p(\omega)$, this requires that (Kazuo Makishma 1988)

$$\overline{p(R\omega)} = \overline{c(R)p(\omega)} \tag{1.2}$$

This should be held for any positive number R and any positive value of ω. In this formula $c(R)$ is a positive function and with the condition $c(1) = 1$, and the bars refer to the ensemble average. Take a logarithm of formula (1.2) and let

$$P(\omega) = ln\overline{p(\omega)}, \tag{1.3}$$

and

$$C(R) = ln\overline{c(R)}, \tag{1.4}$$

then it can be written as

$$P(R\omega) = C(R) + P(\omega), \tag{1.5}$$

again let

$$R = 1 + x \tag{1.6}$$

where the x is an infinitesimal variable, (1.5) becomes

$$x\omega P'(\omega) = C(1) + xC'(1) \tag{1.7}$$

Then let $\beta = -C'(1)$, we obtain

$$P'(\omega) = -\beta/\omega \tag{1.8}$$

where $C(1) = 0$ condition is used.

Integrate (1.8), we can obtain

$$P(\omega) = -\beta ln\omega + b \tag{1.9}$$

b is the arbitrary constant. Let $B = e^b$, then

$$\overline{p(\omega)} = B\omega^{-\beta} \tag{1.10}$$

so the power spectrum is in the form of power law.

Because of the power law form of the power spectrum, a self-similar variation has several peculiar properties. The power would diverge at high frequency limit if $\beta < 1$, at low frequency limit if $\beta > 1$, and at both limits if $\beta = 1$. Since the actual variance should not diverge we expect $\beta > 1$ at sufficiently high frequency and $\beta < 1$ at sufficiently low frequency.

There are two parameters which connect the variability timescale. The first parameter, the shortest variability timescale T_{min} on which the variability can occur, is the light travel timescale, and the second parameter is the efficiency η which measures how much mass is converted to energy.

For black hole accretion we expect the minimum timescale for flux variation, T_{min}, to be greater than the light travel time across a distance equal to the Schwarzschild radius of the black hole

$$T_{min} > \frac{2GM}{c^3} \sim 1000 M_8 \ s \tag{1.11}$$

where M_8 is the black hole mass in units of 10^8 solar masses. We see here that the shortest timescale variability scales with the mass of the black hole.

The efficiency, η, can be expressed by(Cavallo and Rees 1978)

$$\eta \geq \frac{5\Delta L_{43}}{\Delta t} \tag{1.12}$$

where ΔL_{43} is the change in luminosity in units of 10^{43} erg s^{-1}. Note here, it is the total luminosity that changes in the time interval Δt. If a variation extends through other wavebands, then the measured change in X-ray luminosity provides a lower limit for efficiency η. When the black hole model is an isotropic model, it requires $\eta < 10\%$. Those sources with value $\eta > 10\%$ imply non-isotropic or rotating models(McHardy, 1985). The maximum efficiency η is directly connected to the shortest timescale which in turn relates to the central region of the system. Both parameters are useful in understanding X-ray variability.

PART 2

It is well known that the X-ray producing region, the inner part of the accretion disk relevant to Active Galactic Nuclei, is subject to

many instabilities. It is believed that this region suffers instabilities of thermal and viscous and hydrodynamical natures (Abramowicz et al, 1990) such as shocks, magnetic flares, convective cells, blobs of locally denser matter and so on.

Some observational effects (Pounds and Turner, 1986) imply that the inner part of the accretion disk is more like a collection of lumps distributed on the surface of the accretion disk around the central black hole. These phenomena will cause the brightness fluctuations of the source.

Hawley (1987) has done particular numerical work about this. He shows that when some perturbation grows up the disk will break up as a group of planets moving around black hole.

Unfortunately, at present, there is no theoretical model which can describe this accurately. Therefore it seems reasonable to adopt a phenomenological model. In this dissertation, we approximate this non-stationary properties as a group of "hot spots" spread randomly on the surface of the disk, with certain prescribed distribution functions for their life time $\tau_s(r)$, brightness $I(r)$, surface number density $n(r)$, and the characteristic size ΔD. Because of the rotation symmetry, all of these quantities depend on r, the location of the spot.

The concept of "hot spot" is initially put forward by Syunyaev (1972) based on the instability theory of accretion disk. He suggests using this model to explain the characteristic time variation in some galactic X-ray sources, say Cyg X-1, and predicts that this "hot spot" should exhibit a characteristic quasi periodic variability in X-ray band. A possible mechanism for the creation of "hot spot " is given. When the mechanism for

transferring angular momentum outward has a low efficiency, turbulent convection processes will lead to hot material carried out from inner layer to the surface of disk, and formation of current sheets through annihilation of magnetic line of force will lead to solar- type flares. Both of these mechanisms tend to produce "hot spots" on the surface of the disk. In these cases gravitation is the source of energy radiated at the spots. The life time of the spot depends on the ratio of the development of the current sheet or on the cooling rate for a convective spot, and it may considerably exceed rotation period of spot. But we know the power spectrum for AGN is featureless and the periodic properties in short time scale (hours -months) are rarely found.

Those "spots"of large size produced by the instability can not survive on the surface of the accretion disk, especially inner part of the accretion disk, for a long time, say several orbital times. Instead, they will be smeared out very quickly, because the large gradient of the angular velocity exists there. When a spot with a relatively a smaller size moves around central black hole at relativistic speed, the intensity of the X-ray photons arriving at the detector will change periodically at the orbital frequency of the spots, due to the Doppler effect, gravitational focusing, and the geometry of the disk. As a result of the statistic property of the spots, X-ray intensity from considered sources will contain the information of statistics, orbits of the spot and the geometry of disk. Rotation can play a very important role in X-ray variability when these spots can survive a few orbital periods. When the disk is seen almost face-on (small viewing angle), the observed variability may only reflect the intrinsic changes due to instabilities, but not the rotation of the disk,

whereas when the disk is seen at large viewing angle, the intensity of radiation emitted by the spots will be strongly amplified and reduced by the relativistic Doppler effect, and gravitational focusing. In addition, if the spots are deep in the funnels of the accretion disk, occultation occurs as well. Therefore, though the spots themselves are very important to the understanding of variability, the rotation effect can also play an important role in AGN time variability.

If the rotation law of disk at a given radius is not too different from Keplerian one

$$\omega \sim 7 \times 10^4 \left(\frac{M}{M_\odot}\right)^{-1} \left(\frac{r}{r_G}\right)^{-3/2},$$

then the observed short term variability reflecting the accretion disk rotation corresponds to the variability frequency range (in Hz)

$$10^{-5} < \omega < 10^{-3}.$$

The instability works efficiently only inside certain radius of accretion disk, i.e. in the radiation pressure dominant region (Shakura and Syunyaev 1976). The disk is smoother as one goes out radially. This should offer a "knee" behavior at the lower frequency range in power spectrum, while the inner edge of disk offers a roll-off frequency at the higher end. The variability between these two frequencies would be affected by spots. So we expect its power spectrum would take different forms as the frequencies are crossed. Observation shows that these two frequencies, appearing in galactic X-ray sources, are characterized by "knee" frequency and quasi-periodic oscillation (QPO) frequency. But for AGNs the data are not so good and complete as to be able to give us any hint about these two frequencies, probably the observation for

AGN is still within the range of the frequencies.

In this dissertation, we use the "hot spot" model to explain the self-similar behavior of AGNs. The spot production and decay processes might themselves deserve some detailed and rigorous analysis. However, assuming these properties have already been given, we will concentrate on how spots statistics and orbital motion of spots can change the variability in the frequency range corresponding to possible orbital frequency.

In Chapter 2 we will have a brief review of observational data for long-time and short-time AGN variability and also of the galactic X-ray sources. In the final part of this chapter we will summarise those important points which we think are related to the "spot " model.

In Chapter 3 the "hot spot" model will be discussed. First, calculations of flux for single spot with relativistic orbital speed will be presented. Secondly, time variation due to many spots will be discussed. Finally, simulated lightcurves and their power spectra under an ideal condition will be shown.

In Chapter 4, we will make a summary of our results, point out the restriction of the model and outline our future work.

Chapter 2

X-ray variability of AGN and galactic X-ray sources

The X-ray variability of AGN is expected to provide a strong diagnosis of physics about central region, such as accretion mechanism and the central mass of the black hole both of which are fundamental to the understanding of AGN phenomenon. Many well-known deductions are drawn from the observed variability.

For long timescale, the fact that the data are limited, the observation is non-equally spaced and the converting of all fluxes measured by different satellites to something unified and reliable is extremely difficult prevents us from finding some curious phenomena such as "knee" behavior in the low frequency end of the spectrum as seen in galactic X-ray sources Cyg X-1, which is supposed to be connected to viscous time scale containing information on the surrounding accretion disk.

A great deal of interest has been raised in connection with the study of rapid X-ray variability in AGN, owing to the short term variability

timescale and the high energy involved which imply large values of $\frac{dL}{dt}$. Usually the fast variability is often associated with an orbit time of matter moving around central black hole or with the light travel time across the central engine. Important constraints can be derived on the energy conversion mechanism, its efficiency η (Cavallo and Rees,1978), and the physics of central region.

Prior to the launch of EXOSAT the low sensitivty of X-ray detectors and short continuous observations afforded by low-earth-orbit satellites had given a rather poor picture of AGN' X-ray variability in its short trend. The EXOSAT observatory revolutionized our view of short timescale variability by providing about 4 days uninterrupted observation, together with the large effective area of its Medium Energy detectors. It provided the opportunity to seriously investigate the X-ray variability of cosmic X-ray sources on timescales from milliseconds to 3-4 days. As a result of this , power spectrum and "fractal" analysis techniques were applied for the first time to the X-ray light curves of Seyfert 1 galaxies (Lawrence et al. 1987; McHardy and Czerny 1987; Pounds and Turner 1988).

2.1 Survey of long-time AGN variability

Prior to the launch of EXOSAT long-timescale X-ray variability (months -years) had been relatively reasonably established compared to short-timescale in AGN (McHardy, 1985).

One of the best samples is the object B21218+ 305(Wilson et al., 1979), which shows long term variability in its light curve spanning four

years and showing some possible outbursts. The X-ray outburst took place at the beginning of 1974 while the optical one was a hundred days later.

The object Cen A in the radio galaxy (McHardy, 1985) is another good sample. This low-luminosity X-ray source($L_{2\sim 10kev} \sim 10^{41} ergs^{-1}$ in its low state) increased in brightness by a factor of more than 5 from 1970 to 1973, and returned to a low state by 1977 where it remained until 1979 when it again brightened by $\sim$ factor 5. Superimposed on these gradual variations were more rapid variations with timescale of $\sim$ 10 days. The examinations of rapid changes confirm that long timescale variability is not related to any fundamental parameter associated with the central black hole, such as its mass. It is more likely to be associated with changes with fueling rate, which could be linked to the instabilities in the cooling flow.

However, in general, long-term trends are not common. Marshall et al (1981) have studied the long-term light curves of 28 AGNs which are bright enough to be detected. The observation period is from 30 days to 5 years. The only sources from which Marshall et al detected a possible trend are the Seyfert 2 galaxy NGC 526A, the QSO 3C273 and Seyfert 1 galaxy NGC 3783. They conclude that there is definite evidence for irregular variability, at about a steady level, by up to factor of 2 on timescale $\leq$ year $\sim$ 50% of AGN they have studied. Sometimes these irregular variabilities could be attributed to $\sim$ few days outbursts in the sources, which, they think, may be the case for much of the variability. But in general the data are insufficient for a detailed analysis of the character of the variability.

In addition, some of the light curves of AGN, especially the optical light curves for BL lac objects, show not only outbursts but also deep minimum. Often, after a primary maximum of brightness, there is a general decayed second maximum. The second maximum can be delayed after the primary one from days to years. This behavior implies that the mechanism of the outbursts may represent a sort of damped oscillation. Outbursts at different wavelengths are often correlated (Abramowicz, 1988).

It is worth noting that Alloin et al (1986) report the variability of Serfert galaxy NGC 1566. Their data cover 15 years and suggest the occurence of four almost periodic active events (burst), each lasting for about 1300 days, in which the intensity of H_α and H_β lines first increased sharply (in about 20 days) and then decreased again(in a much longer time of about 900 days). The total energy involved in each burst is $10^{51} ergs^{-1}$. The most natural explanation (Abramowicz,et al,1988) of the periodic outbursts of NGC 1566 is the existence of a limit cycle produced by accretion disk instability.

For long timescale, the LE (0.15-1.5 kev) and ME(2-10 kev) fluxes vary more or less together, not always by exactly the same amplitude, though. For example, the ME flux from Seyfert 1 galaxy Fairall 9 decreased by a factor $\sim$2.2 between October 1983 and October 1984 while the LE flux decreased by a factor of $\sim$3.5. In the case of Mkn 335, a source with strong soft excess, the ME and LE fluxes both increased by a factor $\sim$6 between November 1983 and December 1984. There are many more examples of reasonably correlated long timescale ME and LE variability, e.g. NGC526A, the N-galaxy 3C371 and 3C120. McHardy

(1989) suggests that the ME and LE emission regions are spatially separated.

More recently, after meeting difficulties in finding characteristic time scale of X-ray variability in short trend which is expected to reveal information about the central mass, Roberto G. Abraham et al(1989) investigated the power spectra for long timecale, trying to find the evidence of characteristic timescale at low frequencies, in analogy with low frequency roll-over observed in the power spectrum of galactic black hole candidate Cyg X-1. They constructed long timescale medium energy light curves(spanning$\sim$ 10 years) for a number of AGNs, using data primarily from EXOSAT, Einstein, HEAO-1 and Ariel V. They argued that in addition to high frequency roll-over in AGNs' power spectra which avoid an implied infinite mass to energy conversion efficiency, there should exist another roll-over (flattening) at low frequencies. While this low frequency roll-over may well tell us some information about the central black hole, it may well correspond to some sort of viscous timescale, which, in turn, indicates something about the physics of a surrounding accretion disk. They found that the power spectrum of NGC 4151 is similar to $1/f$ noise on long timescales, and that $1/f^2$ noise best describes the short timescale variability. However, they have not observed the sharp turnover seen in Cygnus X-1.

2.2 Short-time variability

Prior to the launch of EXOSAT, variability in AGN on time scales less than $\sim$12 hours was generally thought to be rare. The result of the

HEAO-1 A2 study of some 38AGN were summarized by Tennant and Mushotzky (1981) in a paper entitled "The Absence of Rapid X-ray Variability in Active Galaxies". However, the realization that rapid variability was not so rare led to the allocation of several long continuous EXOSAT observation. Gradually encouraging signs started to appear.

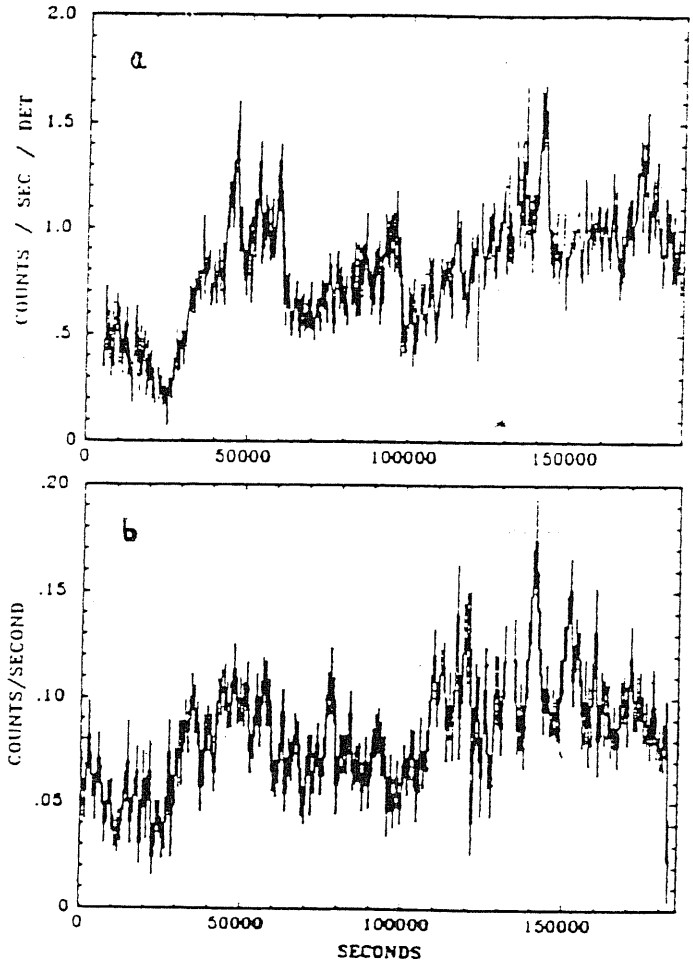

Figure 2. Background subtracted ME and LE light curves of MCG-6-30-15 during 29-31 January 1986 (Pounds and Turner, 1986)

Investigations tended to focus on finding periodicity through which, it was hoped, some information about the central mass could be obtained. However, nothing was found.

The first clear example of rapid X-ray variability from EXOSAT observation was of the low luminosity Seyfert NGC 4051(Lawrence et al,1985). During the 8.5 hour observation large amplitude variability on timescale of ≤ 1 hour was detected, and this confirmed and considerably extended a similar result from an Einstein Observatory IPC observation.

One of the best detections of rapid variation in AGN flux is MCG-60-30-15 , a typical Seyfert galaxy with luminosity $L_{2-10} \sim 10^{43} ergs^{-1}$. A relative short EXOSAT spectral survey in June 1984 revealed continuous variability, well-correlated in both ME and LE detectors on timescale down to one hour (Pounds et al,1986). To examine this Seyfert in great detail, a further EXOSAT observation was carried out in January 1986 lasting for over two days, the source again bright and strongly variable. Figure 2 shows the ME (2-6kev) and LE (0.15-1.5kev) lightcurves with the background subtracted.

Two particular strong "outbursts" were seen $\sim 9 \times 10^4 s$ apart but the variability was essentially continuous. Close examination shows fact-of-two changes in $\leq 1000s$, Figure 1b shows the independent LE lightcurve, whose visual comparison with Figure 2a shows the strong but less than perfect correlation. Figure 3 is the power spectrum of NGC6-30-15 's lightcurve which shows a *power law* form with slop β about -1.2.

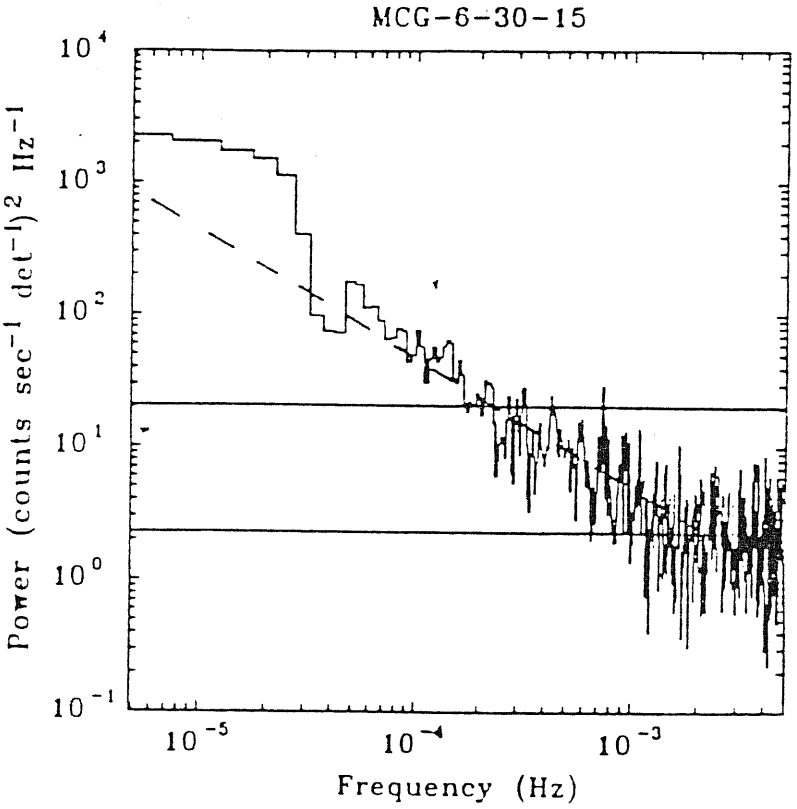

Figure 3. Power spectrum of 2-6 kev light curve of MCG-6-30-15. Dashed line is for f^{-1} and horizontal lines at power levels of white noise and this plus 5 σ (Pounds and Turner, 1986).

The traditionally brightest Seyfert galaxy NGC 4151 shows a markedly different behavior to MGC 6-30-15, a source of similar X-ray luminosity. Figure 4 shows two of the longest EXOSAT observations in which the most evident variability is slow trend, rather than a rapid fluctuation. Its power spectrum (Figure 5) expresses this character. The power spec-

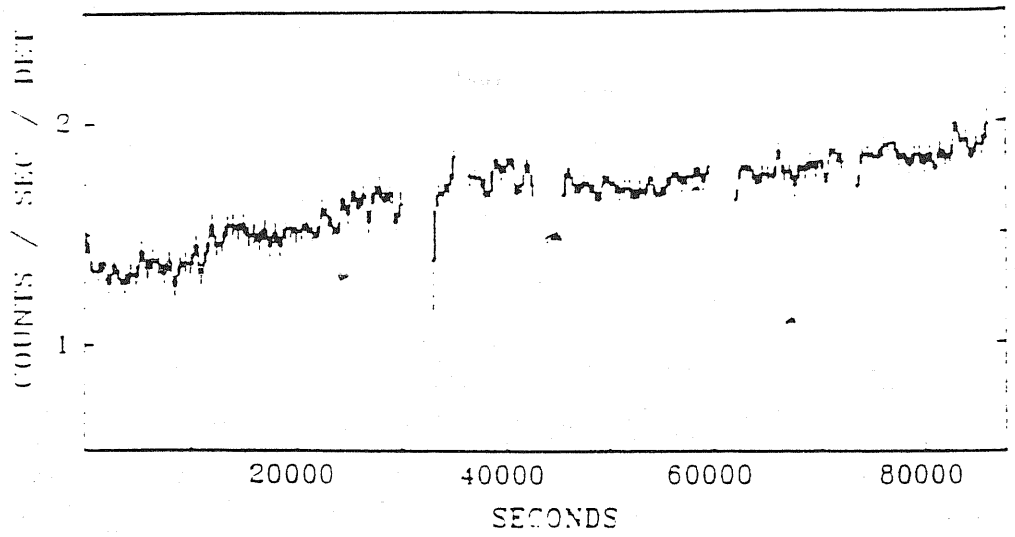

Figure 4. Background subtracted 2-6kev light curve of NGC 4151 during July 1983 (Pounds and Turner, 1986).

trum is of slope of -2, little power is seen with frequencies higher than $\omega \sim 10^{-4} Hz$. This "sluggish" behavior is the typical character of NGC 4151(Perola et al. 1986).

For short term ME AGN observations, McHardy et al(1989) find some correlation between variability amplitude and its X-ray luminos-

ity. Nevertheless, it is still unkown whether the scattering affects the high frequency power or the power spectral slope correlates with other properties of host galaxy.

Because the "long looks" only exist for a small number of well-known bright AGNs, McHardy et al choose the short observation of typical length of 20,000 s for their data material and define the power spectrum nomalization as the variability amplitude at 2×10^{-4}Hz. The variability amplitude is simply the root of the power spectrum at $2 \times 10^{-4} Hz$ which is then normalized by dividing average ME count rate. In order to examine whether the variability is correlated with variability amplitude, they plot a variability amplitude vs luminosity,(see Figure 6).

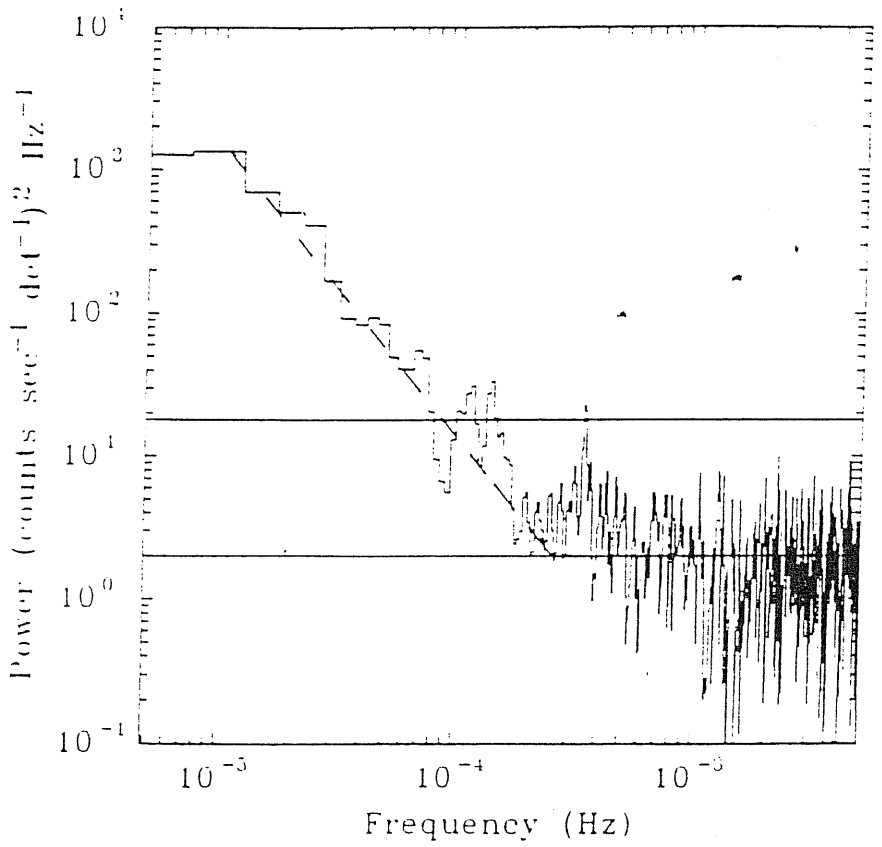

Figure 5. power spectrum of 1983 observation of NGC 4151 dashed line is for f^{-2} slope(Pounds and Turner 1986).

Figure 6 further suggests, based on the assumption that a faster variability implies a smaller central mass, that luminosity scales with the mass rather than that all AGN have the same mass and that the luminosity is mainly a function of accretion rate.

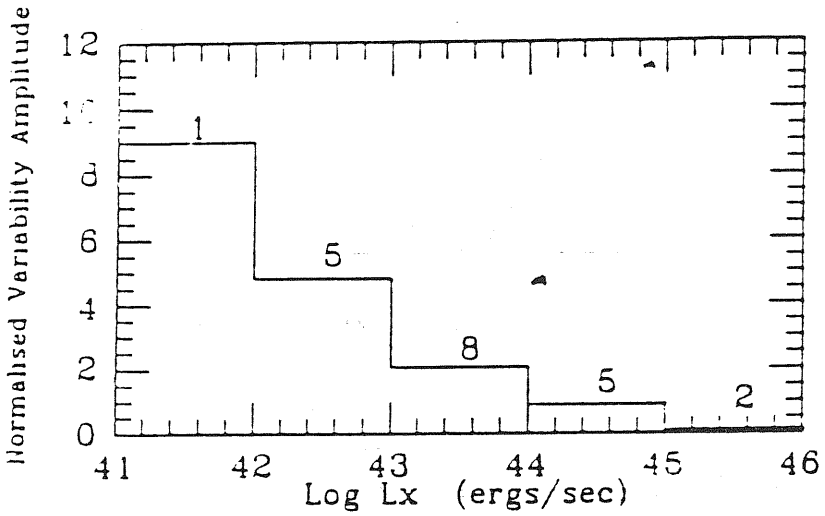

Figure 6 . The average normalized variability amplitude at 10^{-4} Hz plotted as a function of 2-10 kev luminosity. Note that the average normalized variability amplitude in range $10^{45} - 10^{46} ergs^{-1}$ is zero. (McHardy, 1989)

In most cases, the power spectrum in short timescale (hours-days) in AGN is generally well fitted by a *power law*, $p(\omega) \sim \omega^{-\beta}$, with power index ranging from 1 to 2. The power spectrum appears featureless with a possible exception of NGC 6814. Table 1 shows power index β for several sources in different frequency ranges (McHardy, 1989).

In the case of NGC 6814, flare-like features are visible in the light curve and various models of analysis (power spectra, fractals, etc), all pick out a 12,000 second quasi periodicity. Figure 7 is the ME lightcurve

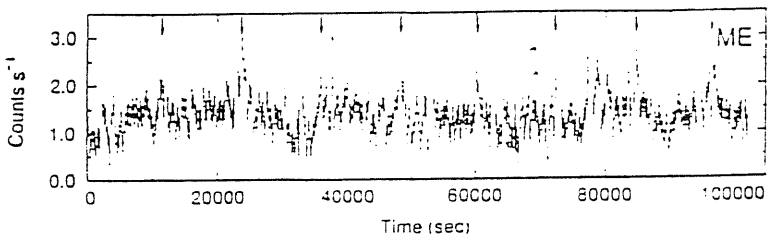

Figure 7. The ME light curve for NGC 6814. The arrows indicate the times of the flares recurring a~ 12000s intervals (Mittaz et al. 1989).

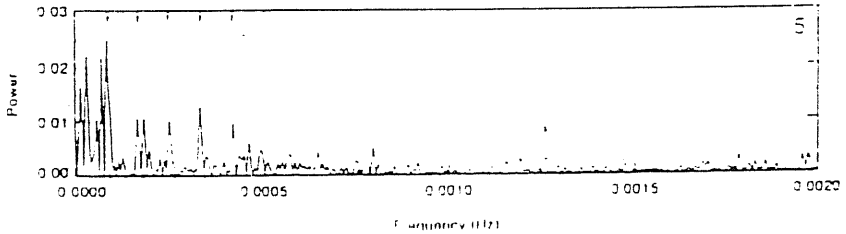

Figure 8 The power spectrum for ME observation of NGC 6814. the peaks are evidence of periodic behaviour: the arrows indicate the ~ 12000s fundamental and its harmonics (Mittaz et al. 1989).

from the observations of NGC 6814. The arrows indicate the flares recurring at $\sim$ 12,000 s intervals, flares and dips occur throughout lightcurves lasting generally from about one to a few thousands seconds. This is the first clear observation of periodic behavior of X-ray energy in an AGN. Figure 8 is the power spectrum of the observations of this object.

The power spectrum of the observation contains a number of prominent peaks which are due to the presence of the small flares in time

line. It seems that the periodic behavior is intrinsic to the source. The identical space in frequency domain of five peaks is marked by arrows. Figure 8 suggests that the positions of the peaks in the power spectrum are harmonically related.

Table 1. ME Power Spectral Slopes

Source	10^{-5} to 10^{-4} Hz	10^{-4} to 10^{-3} Hz
NGC5506	-1.0	-1.9
MCG6-30-15	-1.2	-1.2
NGC4151	-2.0	-2.1
NGC4051	-1.4	-1.4
Mkn335	-1.0	< -1.5
Mkn766	-1.5*	
M81		-1.7

* Average over 10^{-5} to 10^{-3} Hz.

Since the discovery of any characteristic timescale, which could be associated with some important parameters in AGN , for example, orbital period around central black hole, is extremely important from the point of view of determining black hole masses, the periodicity observation becomes crucial. Therefore this sample is further examined.

2.3 Variability of galactic X-ray sources

Figure 9 and Figure 10 are the observed lightcurves and their corresponding power spectra for galactic X-ray sources Cyg X-1 and LMXB

Gx 339-4. They are similar to those in AGN in that their power spectra show a *power- law* form.

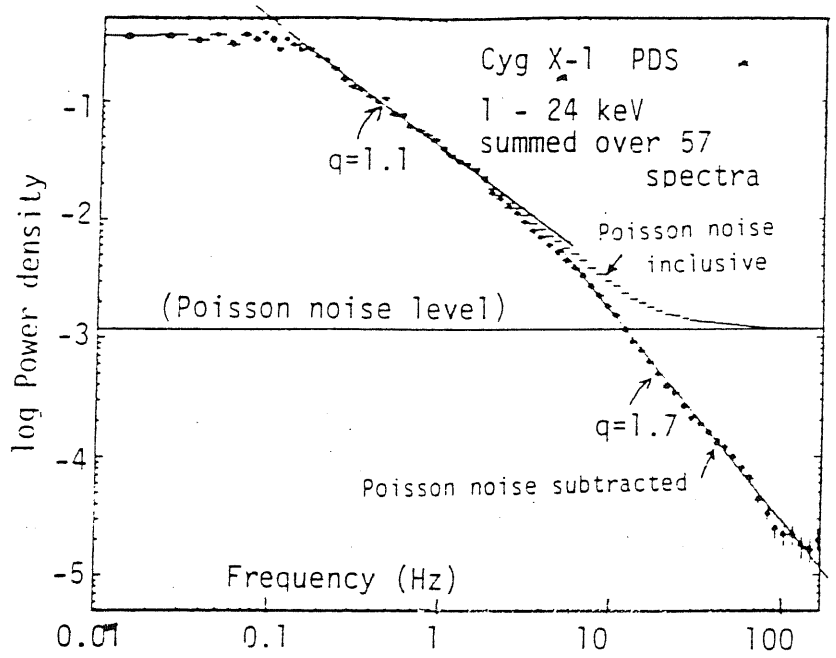

Figure 9. Power spectrum for galactic X-ray sources Cyg X-1 (Makishima, 1989).

A"knee" frequency is seen in the power spectrum of galactic black hole condidate Cyg X-1 (Nolan et al.1981). The knee point is about 0.1 Hz and corresponds to a timescale much larger than the light travel time associated with a black hole of several solar masses (<millisecond). Nolan et al suggest that the knee frequency may be related to clumps

in the accreting material which are produced by the instabilities of accretion disk, and that the disk is unstable only inside certain radius.

Self-similar variation has also been observed in some other galactic sources. Power spectra for several LMXBs observed with Tenma and Ginga together with EXOSAT measurements of many LMXBs consistently indicate that the power spectra slopes of LMXBs are in the range of $1 < \beta < 2$. Most typically β takes the value of 1.4-1.5 in the frequency range of $0.1 - 10$ Hz.

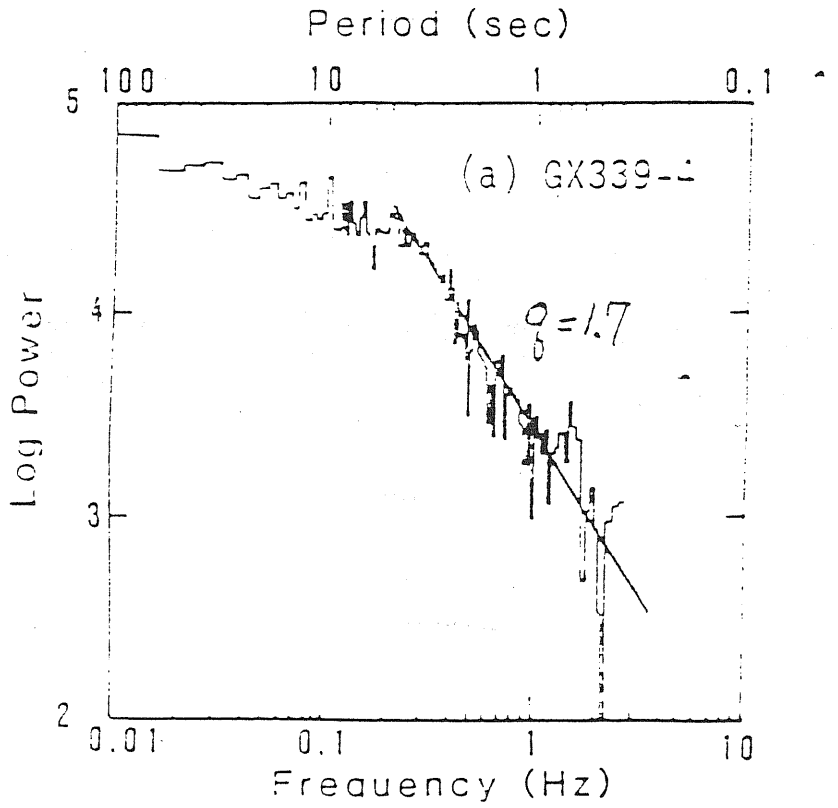

Figure 10. Power spectrum for galactic X-ray sources GX 339-4 (Makishima, 1989).

Unlike CygX-1 the power spectra of LMXB do not show noticeable low frequency flattening at least down to a few mHz. However, the flattening should eventually take place at some low frequencies as their X-ray flux would otherwise diverge. Results from long uninterrupted EXOSAT observation suggest that the flattening occurs at < 1mHz. If so, the knee point frequency for LMXBs is at least two orders of magnitude longer than that of Cyg X-1, GX339-4 and X0331+53. However, this difference is still not clear. Above a few Hz, the self-similar behavior of LMXB often ends up with the quasi- periodic oscillations(QPO).

There are some evidence that the power spectrum rolls off rapidly above QPO frequency. It is thus tempting to interpret the QPO as an end point for self-similar behavior. Figure 11(Makshima, 1988) sums up the power spectra slope measurement of Tenma and Ginga.

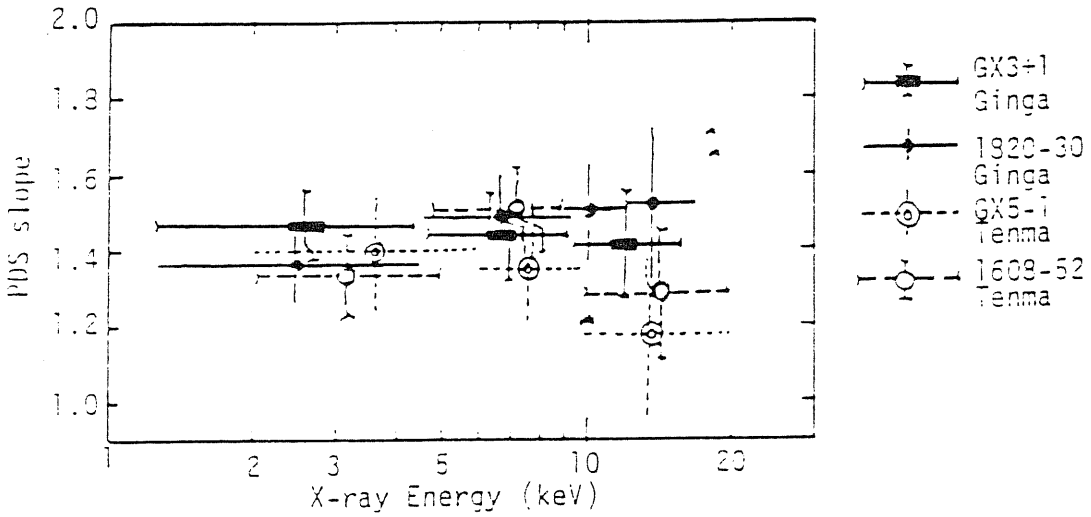

Figure 11. Values of power spectrum slope β measured with Tenma and Ginga, plotted against X-ray photon energy (Makishima, 1989).

2.4 General discussion of the observational data

(a) The slope of power spectrum

The power law forms of power spectra are present in most AGNs, at least, at the observed frequency range. In the range of $10^{-4} - 10^{-3}$Hz all ME power spectra are steeper than -1, which means that the integrated power of high frequency converges. However, for all sources with spectral slopes flatter than -2, the rate of the change of the flux with time gets faster as one goes to shorter timescales.

Any instability responsible for the creation of spots should not have the same strength for different regions which correspond to different orbital frequency range. So we would expect the phenomenon that power spectrum goes flatter as one approaches low frequency to reflect physics of rotation law and statistic properties of spots, such as the number distribution of spots $n(r)$, the spots size distribution $\Delta D(r)$, the spots brightness distribution $I(r)$, and the spots life time distribution $\tau_s(r)$.

(b) The correlation between variability amplitude and luminosity

As far as this problem is concerned, we may have different arguments. Does the fact that variability amplitude is inversely correlated with luminosity imply something about geometry of accretion disk, especially the inner part ? At least, some people believe so. When explaining the absence of rapid variability for NGC 4151 (a bright source), Pounds and Turner (1986) suggest that the viewing angle of the inner part might be

crucial.

Large viewing angle would introduce large variability amplitude in its energy flux according to "hot spot" model. The problem is that we do not know the geometry of the inner part at the moment (Pounds and Turner). It would be very interesting to have a clear picture of this. Recently, some possible evidence for a significant iron k-emission line (6.4 kev) in some AGN X-ray spectrum (Pounds et al 1989, Fabian and Rees 1989, Nandra etal 1989) implies that if a disk is involved in AGN, future medium- to high-resolution X-ray spectroscopy of the iron line will provide the possibility of measuring the disk inclination angle of the inner part.

(c) On ME and LE components

There are several sources which are bright enough in the LE telescopes for the variability of 0.15-1.5 kev band.

In the case of NGC 4051, the fact that the overal spectrum can be fit reasonably well by a single power law indicates that much of the flux detected in 0.05-1.5kev band is simply an extension of ME flux. However, in the case of NGC6-30-15, and particularly in the case of Mkn 335, both the LE lightcurve and the energy spectrum indicate the presence of substantial soft components, although the ME and LE show a substantial correlation. Variation sometimes shows up strongly in one band but only marginally in the other. Both LE and ME emission dominant events occur. These imply the LE and ME emission regions are spatially separated but closely related.

It is clear that in the frequency range of $10^{-5} - 10^{-4}$ the LE power spectrum is *steeper* than the corresponding ME ones. This implies that

there is less high frequency variability in LE components than that in the hard one.

ME photon emission region should be closer to central black hole than LE one, and the spots which are closer to center should have higher orbital frequency. Therefore, ME light curve would show strongly rapid variability while the LE shows it less strongly, the result of which is that LE power spectrum is steeper than that of ME.

(d) The similarity between AGN and galactic X-ray sources

Both AGN and galactic X-ray sources exhibit self-similar behavior. As has been mentioned in the introuctin, we also expect "knee" frequency and roll-off frequency in AGN's power spectrum. Possibly, in the power spectrum of NGC 5506 at frequency range of $10^{-9} \sim 10^{-7}$Hz a flattening behavior could be found. There might exist a "knee" frequency in its low frequency range.

The variability of galactic X-ray sources show strong similarities to AGN in aspects of power law spectra, probably "knee" and roll-off frequency. These similarity patterns are quite apparent when one realizes that the corresponding timescales must differ by a factor $\sim 10^8$ because of mass difference(Abramowicz, 1989). This indicates a very similar physical mechanism of variability both in Active Galactic Nuclei and in galactic X-ray sources.

Either AGN or most of galactic X-ray sources are believed to be powered by accretion disk. The similarity between them might be related to the presence of "hot spot" on the surface of accretion disk.

Chapter 3

A model for short-time X-ray variability

Now let us turn to the theoretical part. In this chapter, we start from a single spot model, then study time variability due to many spots in the discussion of which the power spectrum method will be introduced, and finally show the numerical simulated light curves and power spectrum under some given condition.

3.1 Single spot model

To know the behavior of a large collection of spots, we will start from a single spot. Once the behavior of such a point source is well understood, the contributions from an arbitrary shaped spot can be obtained from the single spot through integration over the spot surface. What is more, the collective behavior of all spots is a result of joint contributions from all individual spots. Further, a single spot offers the largest variation

on the statistical basis and an isotropically radiating sphere is identical to a point source mathematically.

The light curves generated by a finite-sized star, orbiting in the equatorial plane around an extreme Kerr black hole, have been computed by Cunninham and Bardeen (1973) using a hybrid numerical and graphical method (see also Asaoka, 1989 for a more recent, pure numerical approach). Here, we will not consider the general relativistic effects on the light trajectories, as this will enable much of the calculation of a light curve to be done analytically. In fact, as long as the viewing angle is not so large, the relativistic correction can not change our result significantly.

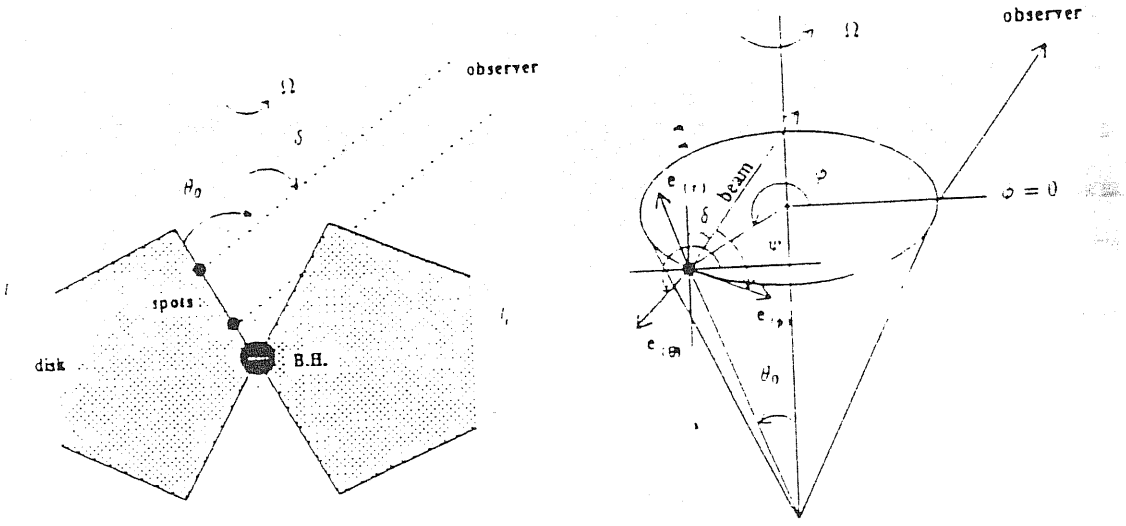

Figure 12. The disk has height ℓ, funnel opening angle θ_0 and rotates rigidly with angular frequency Ω. The line of sight of the observer at infinity makes an angle δ with the axis of rotation. The spot is located at height ℓ, and co-rotates with the disk.

Let us consider a single, point-like spot. We shall treat the spot as a tiny sphere radiating isotropically in its own rest frame. The shape of the disk will be approximated by four conic surfaces as shown in Figure 12. The inner cone (the funnel) has an opening angle θ_0 and the disk hight is l, the spot is located at hight l_s on the funnel wall and rotates around the black hole with angular velocity Ω, the observer is at angular position $\phi = 0$ with viewing angle δ.

In a non-relativistic situation, eclipses of spot produce a square-wave-like light curve. The width of the squares decreases as the viewing angle increases, until a critical angle δ_c is reached for which all the light from the spot is blocked by the disk wall and the width turns to zero. However , in full relativistic case, the light curve will be modulated strongly by Doppler beaming and gravitational focusing (if the observer is close to the equatorial plan). In addition, a spot with viewing angle greater than δ_c may still be visible due to gravitational bending of the light. Here, for simplicity, we do not consider the gravitational effect on photon trejectory, therefore our result emphasizes more on Doppler beaming.

A spot with observed intensity I_{obs} which occupies a solid angle $\Delta\Pi$ has the observed energy flux

$$F_{obs} = I_{obs}\Delta\Pi \tag{3.1}$$

It is well known (see, e.g., Misner, Thorne and Wheeler, 1973) that the volume in phase space, V, (measured in any local Lorentz frame) is conserved along photon trajectory(Liouville theorem in curved space time) though the phase space region it occupies changes. This leads to

Collisionless Boltzmann equation which gives

$$I_\nu/\nu^3 = \text{constant} \tag{3.2}$$

where I_ν is specific intensity of radiation at given frequency ν measured in a specified local lorentz frame.

The total intensity of a light source, integrated over its effective frequency range, is changed by a factor of the fourth power of the redshift factor, g,

$$I_{obs} = g^4 I_{em} \tag{3.3}$$

The redshift factor is, by definition, the ratio of the observed energy of a photon, E_{obs}, to the energy of the photon in its source's rest frame, E_{em},

$$g = E_{obs}/E_{em} \tag{3.4}$$

For an observer at rest at infinity its four-velocity is approximately

$$\vec{u}_{obs} = (1,0,0,0) \tag{3.5}$$

(Here and in the following, the spherical coordinate and the geometric unit in which $G = c = 1$ will be used). The observed photon energy, in terms of the four-momentum $\vec{P}$ of the photon, is

$$E_{obs} = -\vec{u}_{obs} \cdot \vec{P} = -P_t \tag{3.6}$$

and the energy measured at the rest frame of the spots is

$$E_{em} = -\vec{u}_{em} \cdot \vec{P} \tag{3.7}$$

Choosing Schwarzschild metric

$$ds^2 = -\left(1 - \frac{2M}{r}\right) dt^2 + \left(1 - \frac{2M}{r}\right)^{-1} dr^2 + r^2(d\theta^2 + \sin\theta^2 d\phi^2) \tag{3.8}$$

Setting up an orbiting orthonormal tetrad on the considered spot,

$$\vec{e}_{(\mu)} = \Lambda^{\alpha}_{(\mu)} e_{\alpha}, \qquad \mu, \alpha = t, r, \theta, \phi \tag{3.9}$$

which comoves with the accretion disk. The time leg of the tetrad is the four-velocity of the spot, so its components can be expressed as

$$\Lambda^{t}_{(t)} = \frac{1}{\sqrt{(1-\frac{2M}{r})(1-v_s^2)}}, \tag{3.10}$$

and

$$\Lambda^{\phi}_{(t)} = \frac{\Omega}{\sqrt{(1-\frac{2M}{r})(1-v_s^2)}} \tag{3.11}$$

where

$$v_s = \frac{\Omega l_s \tan\theta_0}{\sqrt{1-\frac{2M}{r}}} \tag{3.12}$$

is the velocity of spot measured in a local non-rotating frame and

$$\Omega = \left(\frac{d\phi}{dt}\right) \tag{3.13}$$

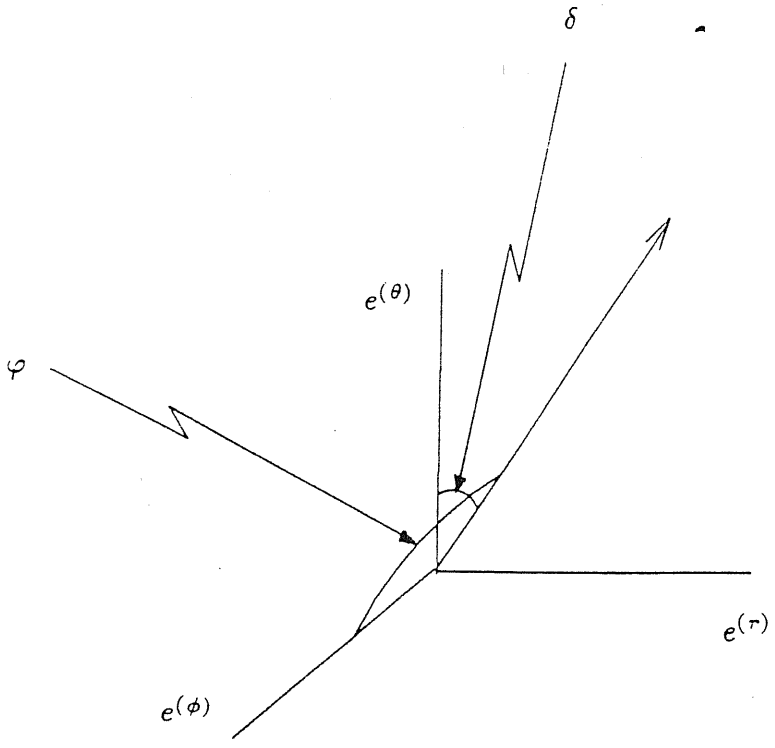

Figure 13. Orbiting orthonormal frame. Arrow points photon emitting direction and $e^{(\phi)}$ represents moving direction of emitting matter.

is its angular velocity. Choosing $\vec{e}_{(\phi)}$ to be orthonormal to $\vec{e}_{(t)}$, pointing in the ϕ direction in the comoving frame, and with the condition that the length of the vector is unit, we obtain

$$\Lambda_{(\phi)\phi} = \frac{l_* \tan\theta_0}{\sqrt{1-v_s^2}}, \tag{3.14}$$

$$\Lambda_{(\phi)t} = -\Omega\Lambda_{\phi(\phi)}. \tag{3.15}$$

The remaining two space-axis are chosen to be in the r and θ direction and their components are

$$\Lambda_{(r)r} = \sqrt{1-\frac{2M}{r}} \tag{3.16}$$

$$\Lambda_{(\theta)\theta} = r. \tag{3.17}$$

The energy of emitted photon in the rest frame of spot can, therefore, be written as

$$E_{em} = -\vec{u}_{em}\cdot\vec{P} = P^{(t)} \tag{3.18}$$

so the g, redshift factor, can be found through

$$\begin{aligned} g &= \frac{E_{obs}}{E_{em}} \\ &= -\frac{P_t}{P^{(t)}} \\ &= -\frac{P_t}{\Lambda^{(t)}_{\mu} P^{\mu}} \end{aligned}$$

Using above equations we can find

$$g = \frac{\sqrt{(1-v_s^2)(1-\frac{2M}{r})}}{1-\Omega L} \tag{3.19}$$

where L is the impact parameter of photons around z-axis. L can be written as

$$L = -\frac{P_\phi}{P_t} \tag{3.20}$$

The redshift factor is independent of both energy, P_t and the angular momentum, P_ϕ, of photon, it only relies on their ratio, i.e. the direction in which photon is emitted. The impact parameter L is periodically changed as the spot moves around the central black hole. When the spot moves towards the observer, g is amplified and the measured frequency of the photon is blueshifted; when the spot recedes from the observer, the measured frequency is redshifted.

Further if we assume that the angle between the photon beaming and the motion of the spot (tangent to the orbital motion) is ψ (see Fig. 13)

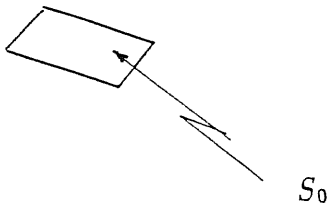

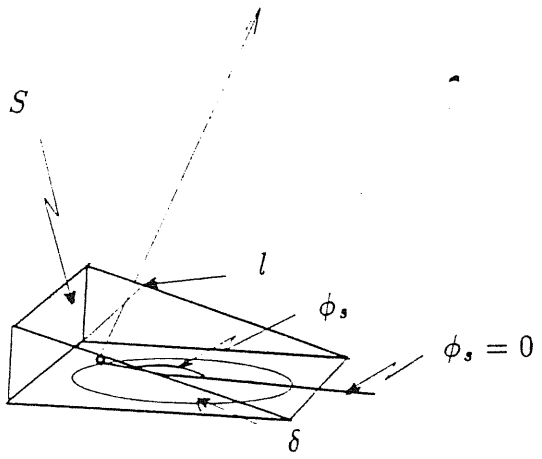

Figure 14. Those photon rays crossing line l have the same delay time Δt. S_0 is observer's photographic plate which is parallel to plan S.

$$L = -\frac{P_\phi}{P_t} = -\frac{\Lambda_{\phi(\mu)} P^\mu}{\Lambda_{t(\nu)} P^{(\nu)}} \tag{3.21}$$

and it can be expressed as

$$L = \frac{\Lambda_{\phi(t)} + \Lambda_{\phi(\phi)} \cos\psi}{\Lambda^t_{(t)} + \Lambda^t_{(\phi)} \cos\psi} \tag{3.22}$$

substitute formula (3.10)-(3.17) into (3.22) then we obtain

$$g = \frac{\sqrt{1 - \frac{2M}{r}}}{\sqrt{1 - v_s^2}} (1 + \cos\psi v_s) \tag{3.23}$$

In general relativity, to find the relation between the flux and the photon arrival time t at detector, one has to integrate the differential equations along photon trajectory. Fortunately, it is trivial to integrate these equations in the flat spacetime: all light rays follow straight lines and the travel time is simply the distance the photon travels over speed of light. However, one needs to be careful in that the travel time is different for photons emitted from different orbital positions, unless the disk is seen face-on. This difference in travel time, as compared with photons that would be emitted at the angular position $\phi_s = 0$, can also be calculated very easily (see Fig. 14).

$$\Delta t = \frac{v_s}{\Omega} \sin\delta(1 - \cos\phi_s) \tag{3.24}$$

From Figure 13 we know

$$\cos\psi = -\sin\delta\cos\phi_s \tag{3.25}$$

where ϕ_s relates to the photon arrival time through

$$\phi_s = \Omega t + \phi_c + v_s \sin\delta(\cos\phi_c - \cos\phi_s) \tag{3.26}$$

We have chosen $t = 0$ to be the moment the first photon from the spot arrives at the detector after its creation, and ϕ_c the orbital position of the spot where it is created.

In addition, when the spot is deep in the funnel of the accretion disk the observer can not always see the spot. Now we calculate the value of the $\phi_{eclipse}$ from which the eclipse begins and ends. Imagine that the spot is at rest and an imaginary observer counter-rotates with angular velocity Ω around the spot, forming another cone S_2 with opening angle δ (see Fig. 15). In Figure 15 the cone S_1 represents the wall of

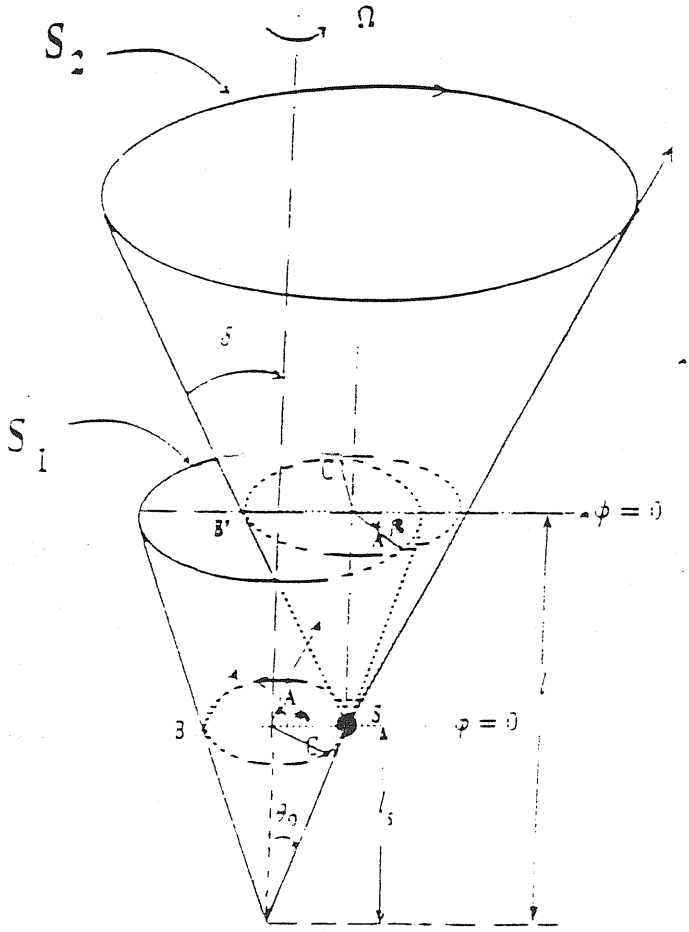

Figure 15. The cone S_1 is the funnel wall. The spot S moves in a circular orbit at height ℓ_s, in the direction ABC. The equivalent observer moves on the cone S_2 in the direction $A'B'C'$. The spot is visible to the distant observer only along the arc ABC.

the funnel. The spot S rotates in a circular orbit with angular velocity Ω on the cone of S_1 in the direction ABC. The light rays emitted at any orbital position must be in the direction $\theta_0, \phi = 0$ in order to reach the distant observer. At the orbital position B the light ray connecting B and the distant observer is equivalent to the line SB' as we can see by turning back the whole configuration by an angle π. Similarly, the light ray connecting A and the observer is equivalent to SA', and the same for C. As the spot completes one orbit the equivalent light rays(SA', SB', SC'.....)will form a cone S_2 with the same angular velocity Ω.

It is clear from Figure 15 that the spot is not visible only for

$$-\phi_{eclipse} < \phi < \phi_{eclipse} \tag{3.27}$$

where $\phi_{eclipse}$ can be computed from

$$\cos\phi_{eclipse} = \frac{1}{2l_s}\left\{(l+l_s)\frac{\tan\theta_0}{\tan\delta} - (l-l_s)\frac{\tan\delta}{\tan\theta_0}\right\} \tag{3.28}$$

Therefore, as a function of the arrival time, the observed energy flux from a spot with infinitely long life time is

$$F_{obs} = \left(\frac{\sqrt{1-\frac{2M}{r}}}{\sqrt{1-v_s^2}}(1 - v_s \sin\delta \sin\phi_s)\right)^4 I_{em}\Delta\Pi \tag{3.29}$$

for

$$\phi_{eclipse} < \phi - 2n\pi < 2\pi - \phi_{eclipse} \qquad n = ..., -1, 0, 1, ... \tag{3.30}$$

if ϕ is outside this range the flux will be zero. In Figure 16 we plot the ratio $I_{obs}/I_s(= g^4)$ in one orbital period as a function of t and viewing angle δ at a fixed disk hight $l = 5r_g$, spot hight $l_s = 2.5r_g$ and

the orbital velocity $v_s = 0.375c$. It is quite clear that as δ increases, the Doppler beaming effect gets stronger, i.e. the rotation effect gets stronger, the time duration when the spot is visible gets smaller. The

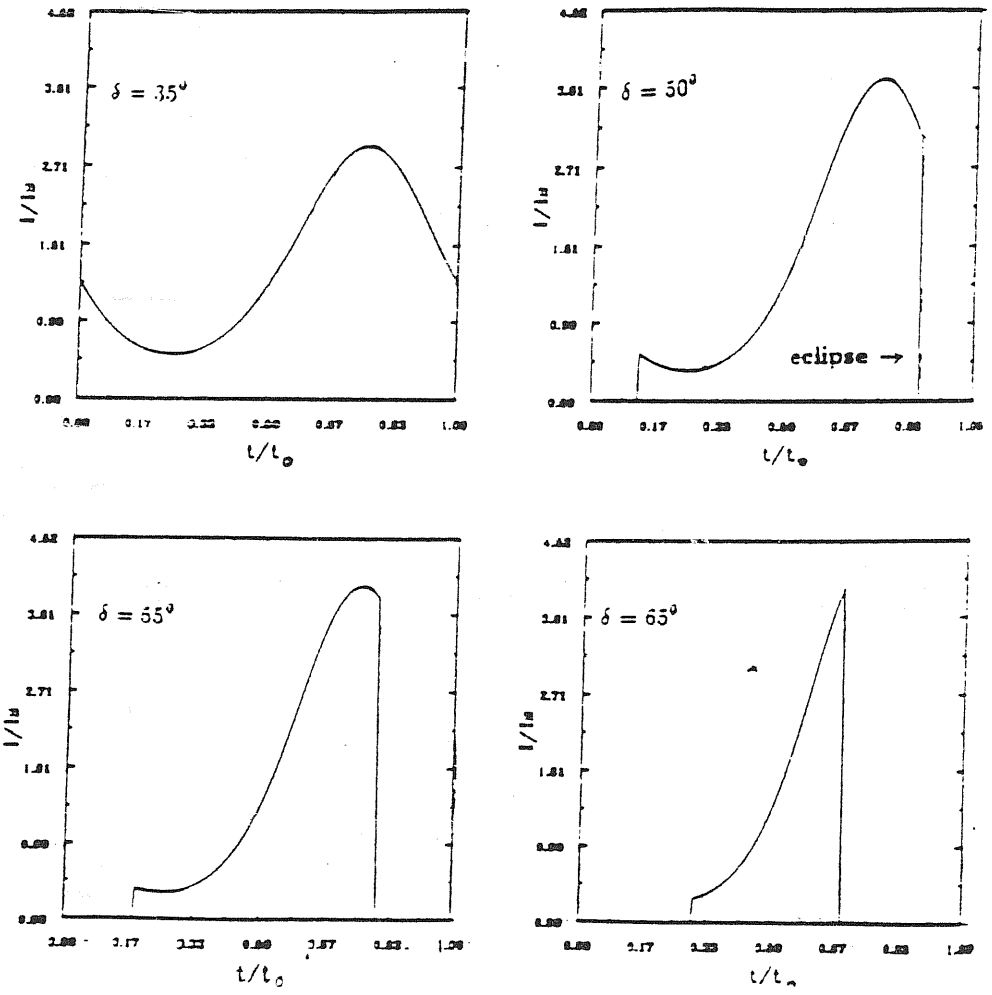

Figure 16. The ratio I_{obs}/I_s is plotted in one period time as a function of t for four different values of δ's: a) $\delta = 35^0$; b) $\delta = 50^0$; c) $\delta = 55^0$; d) $\delta = 65^0$. The disk has opening angle $\theta_0 = 45^0$, height $\ell = 5r_G$ and orbital velocity $v_s = 0.375c$. The spot is located at height $\ell_s = 2.5r_G$.

flux is periodically changed at orbital frequency Ω.

3.2 The power spectrum

Before analysing the power spectra produced by spots, it is worth introducing some basic theory about power spectrum (Rice,1954 and Zhang,et al 1990). Suppose we have a signal $F(t)$ which extends from $t = 0$ to $t = \infty$ then the correlation function $\varphi(\tau)$ of $F(t)$ is defined as

$$\varphi(\tau) = \lim_{T\to\infty} \frac{1}{T} \int_{t_1}^{t_1+T} F(t)F(t+t_0)dt_0 \tag{3.31}$$

where the limit is assumed to exist (here t_1 is arbitrary for stationary processes). The power spectrum is related to this function through

$$P(\omega) = 4\int_0^\infty \varphi(\tau)\cos\omega\tau d\tau \tag{3.32}$$

Further we can write the power spectrum of $F(t)$ in terms of its Fourier transform $S(\omega)$,

$$P(\omega) = \lim_{T\to\infty} \frac{1}{2}\frac{|S(\omega)|^2}{T} \tag{3.33}$$

where

$$S(\omega) = \int_0^T F(t)e^{i\omega t}dt. \tag{3.34}$$

If the lifetime of spots τ_s was finite, there would be many spots during T, and there would also be many spots at any given time. We must add the contributions from all of those spots,

$$P(\omega) = \frac{1}{2}\lim_{T\to\infty} \frac{1}{T}\sum_i |S(\omega; r_i, \phi_i, t_i)|^2 \tag{3.35}$$

Here $S(\omega; r_i, \phi_i, t_i)$ is the Fourier transform of $F_i(t)$ for the i^{th} spot created at the location (r_i, ϕ_i) and time t_i. The summation is over all spots

occurring during time T. If we treat spots creation process to be stationary and spots created at the same radius to be identical, and factor out the constant part of the redshifted intensity from $S(\omega; r_i, \phi_i, t_i)$, and if we convert the summation into integration by introducing the probability function $n(r, \phi_0)$ of the average number of spots created at radius r and azimuthal angle ϕ_0 on the surface of the disk, then we can write

$$P(\omega) = \frac{1}{2} \int \frac{I^2(r)}{\tau_s(r)} |s(\omega, r, \phi_0)|^2 n(r, \phi_0) dr d\phi_0 \qquad (3.36)$$

3.3 Eclipse and power spectrum

The power spectrum for the periodically changing signal is mathematically typical, it should be of many-peaked shape. If $v_s/c \sin\delta \ll 1$, then almost all power, in our case, concentrates on the first peak which corresponds to orbital frequency of the spot Ω . When spots distribute in a narrow region, the eclipse can not change the power spectrum greatly, only controlling the absolute strength of the power, because the eclipsing occurs at the same frequency as that of spot orbit.

To see this, let us consider a simple situation. Assuming that a number of spots appear on the wall of the funnel in a *narrow* range of r, that the probability distribution function for the initial phase is

$$\rho(\phi) = \frac{1}{2\pi}$$

that the first appearence of a spot occurs equally any time during observation and that the characteristic rate of appearence is ν, the distributed portion is (from (3.33) also Rice 1954)

$$P(\omega) = 2\nu \int |s(\omega)|^2 \rho(\phi) d\phi \qquad (3.37)$$

where

$$s(\omega) = \int_{-\infty}^{\infty} e^{-i\omega t} dt$$

For simplicity, we neglect the delay term (this can not introduce relative error larger than 10% when $\frac{v}{c} \sin\delta < 0.25$; when $r = 3r_G$ for Schwarzschild black hole, $\frac{v}{c} \sim 0.33$) and choose $\theta(t)e^{-\frac{t}{\tau}}$ as life time envelope, which expresses that the spot is suddenly turned on and then exponentially decays. $f(t)$ is the square wave function due to an eclipse, and can be written in Fourier series

$$f(t) = 1/2 \sum_{n=-\infty}^{+\infty} b_n e^{in\Omega t}, \tag{3.38}$$

where

$$b_n = \begin{cases} \frac{-2sin(n\phi_{eclipse})}{n\pi} & n \neq 0; \\ \frac{(\pi - \phi_{eclipse})}{\pi} & n = 0. \end{cases}$$

So the energy flux from the spot is

$$\overline{F(t)} = F(t)f(t)\theta(t)e^{-t/\tau} \tag{3.39}$$

From formula (3.7) we obtain

$$P(\omega) = const. \sum_{j=-4}^{4} \frac{c_j^2}{1 + \tau^2(j\Omega - \omega)^2} \left(A_j^2 + B_j^2\right), \tag{3.40}$$

where

$$A_j = (\pi - \phi_{eclipse})/2\pi - \pi \frac{me + df}{e^2 + f^2}$$

$$B_j = \frac{mf - ed}{e^2 + f^2}$$

$$m = sh(\frac{\pi - \phi_{eclipse}}{\omega\tau}) cos\left((j\Omega - \omega)(\pi - \phi_{eclipse})/\Omega\right)$$

$$d = ch\left(\frac{\pi - \phi_{eclipse}}{\Omega\tau}\right) sin\left((\pi - \phi_{eclipse})(j\Omega - \omega)/\Omega\right)$$

$$e = sh\left(\frac{\pi}{\Omega\tau}\right) cos((j\Omega - \omega)\pi/\Omega)$$

$$f = ch(\frac{\pi}{\Omega\tau})sin(\pi(j\Omega - \omega)/\Omega)$$

$$c_0 = 1 \tag{3.41}$$

$$c_1 = c_{-1} = -2v_d$$

$$c_2 = c_{-2} = -3/2v_d^2$$

$$c_3 = c_{-3} = v_d^3/2$$

$$c_4 = c_{-4} = v_d^4/16$$

$$v_d = vsin\delta$$

When the lifetime of the spots which occur on the wall of the funnel is long enough we can see the obvious peaks of the power spectrum, which should occur at

$$\omega = n\Omega, \quad n = 1, 2, 3, ...,$$

Generally, people do not consider the $n = 0$ term. Firstly, this term can never be observed. Secondly, different people treat it in different ways, which alters the real nature of a possible zero component (Lehto, 1989).

The terms related to $j\Omega - \omega$ describe the power density near $j\Omega$, the orbital frequency and its overtones.

The relative strength for each peak is proportional to $v_d^{2j}; j = 0, 1, 2, 3, 4$. From this we can understand that, firstly, the peaks in the theoretical power spectrum are produced by Doppler beaming. When there is no beaming(supposing the viewing angle of the observer is not zero), $v_s = 0$ and there are no distinct peaks in the power spectrum except red noise. The greater the velocity, v_s, of the spot, the more distinct the peaks are in the power spectrum. Secondly, the strength of the

peaks does not depend on the first order or any odd order of velocity. This is easy to understand because the power density of the intensity has nothing to do with the direction of the rotation of the spot. Note that the ratios of hight for the first to the second and the first to the fourth peak are respectively 30 and 10^5 for $v_d = 0.25$. So allmost all power is contained in the first peak.

The shape of the power spectrum depends weakly on the eclipse angle, whereas the amplitude of the eclipse angle changes greatly the absolute strength. We can understand this through formula (3.40) and (3.41). When the lifetime of the spots is long enough, the ratio between peak i and peak j is about

$$\left(\frac{c_j A_j}{c_i A_i}\right)^2,$$

when ω is exactly at the center of the peaks(the ith and the jth),we have

$$A_j = A_i,$$

so the relative ratio between them is

$$\left(\frac{c_j}{c_i}\right)^2,$$

which has nothing to do with the eclipse angle.

But we should note that when spots distribute on the surface of disk in a *broad* range, the power spectrum appears in a power law form (we will see this later), the eclipsing in this case does affect the shape of the power spectrum. For example, when spots are deeper in the funnel wall, this means, for a given observer, larger eclipse is introduced, i.e. the eclipsing prevents faster variability from reaching the observer, which leads to steeper power spectrum.

3.4 Power spectrum due to many "hot spots"

Let us approximate the innermost, X-ray producing region of the accretion disk as consisting of two components: that due to a "disk" component, L_D, and the contribution from all spots, L_S,

$$L = L_D + L_S. \tag{3.42}$$

The steady part, L_D, is to be computed from a disk model, with a noise part added to it; the spots are assumed to have average values as functions of the radius in their brightness, $I(r)$, lifetime, $\tau_s(r)$ and the number of spots per unit radius, $n(r)$. In a statistical sense, the product of the number of spots, within r and $r + \Delta r$, and the spot brightness will correspond to the "strength" of signals, in the frequency range of $\Omega(r)$ to $\Omega(r + \Delta r)$.

When the spots are spread in a wide range of radius, naturally there are no "characteristic" time scales in the resulting light curves, and the power spectra of light curves would show a broad feature. It is straightforward, though tedious, to show (see Appendix) that for axisymmetric $n(r, \phi_c)$,

$$n(r, \phi_c) = \frac{1}{2\pi} n(r) \ ,$$

and an eclipse system,

$$P(\omega) = 1/2 \int \frac{I^2(r)\Delta\Pi^2}{\tau(r)} n(r) dr \sum \alpha_N (v_s \sin\delta)^M J_N(K v_s \sin\delta) G_{\omega - N_1\Omega} G^*_{\omega + N_2\Omega}. \tag{3.43}$$

To write (3.43) in a compact form, we have used a few abbreviations. Their full expressions are given in Appendix. More specifically,

$$K, M, N, N_1, N_2$$

are merely symbolic representations of some integers; α_N corresponds to the N^{th} numerical expansion coefficient; $J_N(x)$ is the N^{th} order Bessel function; G_ω is the Fourier transform of the evolution function $G(t)$ in the spot's own rest frame, and $G^\star_\omega$ denotes its complex conjugate. It is to be noted that $M + N$ is always an even number, which can be understood from the time reversal symmetry of the disk motion.

From this general expression, we can see that, as one would expect, the resulting power spectrum is controlled by the spot number density $n(r)$, the brightness of spot $I(r)$, the lifetime of the spot $\tau_s(r)$, the rotation law $\Omega(r)$ of the disk and the dimension of spot ΔD which is related to the solid angle $\Delta\Pi$. The strength of the repeated feature depends on the projected orbital speed of spots on that ring, $v_s \sin\delta$. When these spots are spread in a large range of radii, the rotation will introduce a broad feature into the power spectrum in the frequency range of the corresponding orbital frequencies.

To study the effects of rotation and statistics of spots on the observed variability, let us consider a simple case where

$$G(t;r) = \begin{cases} 1 & t_0 < t < t_0 + \tau(r) \quad , \\ 0 \ , & \text{otherwise} \quad ; \end{cases} \tag{3.44}$$

and treat the disk to be geometrically thin so that the eclipse will not be considered here. We will also ignore the relativistic corrections to the orbital motion. Since typically,

$$(\Omega r \sin\delta)^2 << 1 \quad ,$$

this will not be a serious limitation even for black hole systems. Then, as long as

$$\frac{1}{\tau} << \Omega$$

we can approximate G_ω as

$$G_\omega \sim \frac{\sin\frac{(\omega-\Omega)\tau}{2}}{(\omega-\Omega)}$$

and the summation in (3.43) will be dominated by the first non-trivial terms (we are not interested in the $\omega = 0$ component here). Therefore, we have

$$P(\omega) \sim \int \frac{I^2(r)n(r)(\Omega r\sin\delta)^2}{\tau_s}\left(\frac{\sin\frac{(\omega-\Omega)\tau}{2}}{(\omega-\Omega)}\right)^2 \Delta\Pi^2 dr$$

and further

$$P(\omega) \sim \left[I^2(r)n(r)(\Omega r\sin\delta)^2\tau_s(r)\left(\frac{dr}{d\Omega}\right)\Delta D^4\right]|_{\Omega=\omega}. \qquad (3.45)$$

From this, we assume that the distribution function $n(r)$, the life time $\tau(r)$, the brightness $I(r)$ and the characteristic size $\Delta D(r)$ do not depend on time and azimuthal coordinate, and their radial dependence can be approximated by the following power law forms -

$$\Delta D \sim r^{\alpha_D} \quad ,$$

$$I_0(r) \sim r^{-\alpha_I} \quad ,$$

$$n(r) \sim r^{1-\alpha_n} \quad ,$$

$$\tau(r) \sim r^{\alpha_\tau} \quad ,$$

and if the disk rotation can also be described in power-law form

$$\Omega(r) \sim r^{-\alpha_\Omega} \quad ,$$

then the resulting power spectrum $P(\omega)$ will also have a power-law form,

$$P(\omega) \sim \omega^{1+\frac{2\alpha_I+\alpha_n-\alpha_\tau-4-4\alpha_D}{\alpha_\Omega}}\sin^2\delta. \qquad (3.46)$$

Now let us discuss these power index, despite the lack of sufficient knowledge. DISTRIBUTION INDEX α_n:

There is no estimation about the possible value both from theory or from observation.

LIFE TIME INDEX α_τ:

It seems physically reasonable that $\alpha_\tau > 0$, which means those spots closer to the central black hole have relatively a shorter life time. It should be noted that if spots are destroyed by shear the life time of spot with a typical dimension ΔD is $\alpha_\tau \sim \frac{r}{\Omega \Delta D}$, then

$$\alpha_\tau \sim 1 + \alpha_\Omega - \alpha_D$$

but we should remember that other physical processes are also important, say, cooling rate for a convective spot, or rate of development of current sheet (Syunyaev 1972).

THE ROTATION INDEX α_Ω:

It is, most probably, close to the Keplerian one, i.e.

$$\alpha_\Omega = \frac{3}{2}$$

However, in general, one should consider a wider range for α_Ω

$$\frac{3}{2} \leq \alpha_\Omega \leq 2.$$

with $\alpha_\Omega = 2$ corresponding to thick accretion disk with constant angular momentum.

BRIGHTNESS INDEX α_I:

Again, there is no theory and observation for it. It is physically reasonable to assume that the spots closer to the central black hole are brighter because the deeper gravitational potential well is there.

DIMENSION INDEX:

There is no theory and observation estimation for it either. It is reasonable that

$$\alpha_D \geq 0$$

i.e. larger size spot can not stay stationarily in inner part of accretion disk.

One interesting consequence of (3.14) is that, for uniform radial distribution of the statistical properties of the spots ($\alpha_n = \alpha_\tau = \alpha_I = \alpha_D = 0$) and for the Keplerian disk ($\alpha_\Omega = 3/2$) the power spectrum has the form

$$P(\omega) \sim \omega^{-5/3} \sin^2 \delta \tag{3.47}$$

It tells roughly how the variability changes with the statistical properties of the spot and the rotation of the disk. It should be mentioned that while this simple power-law form is obtained eclipsing and lorentz factor of orbital speed are ignored. If we put back in the lorentz factor, power spectrum should be flatter than that of (3.47), because the contribution of power from larger orbital frequency is greater.

3.5 Numerical simulations and discussion

To better reveal the effect of rotation and the statistical properties of spots on the observed variability as contained in (3.43), and to avoid the limitations due to the assumptions leading to (3.45), we have also done some simple numerical simulations on light curves and estimated the power spectra directly from these simulated light curves. We approximate the disk to be geometrically thin, so all the spots are orbiting the

central object on the equatorial plane. To generate those light curves, we first assign each spot a randomly selected creation time t_i. We then assign the initial positions r_i of these spots randomly according to their average lifetime $\tau_s(r)$ and the average number of spots per unit radius $n(r)$. The angular position ϕ_i is assigned randomly and uniformly within 2π. The resulting value of the light curve at time t is found by summing the fluxes from all contributing spots and the contribution from each spot is computed using Eq. (3.29). The number of spots on the disk surface at any given time is estimated from the observed amplitude of the variability. Using $\Delta I/I \sim 2$ for a spot at $r = 10M$ [Eq. (2.39)], taking $\Delta I/I \sim 10\%$ as a canonical number from the observation and assuming that $L_S/L_D = 1/3$, we estimate that an average of 100 spots is consistent with observations from the statistics of spots. This is the number we use in the simulation. The innermost orbit ($r_{in} = 6M$) is divided into 32 zones and there are 4000 orbits between r_{in} and r_{out}. The outermost orbit is at $r_{out} = 50M$. Each orbit is divided evenly, with each zone corresponding approximately to the same duration of orbital time for all these orbits.

In Fig. 17 we show the simplest case, with $G(t)$ taking the form of (3.44). The lifetime τ_s is the same for all the spots and it is chosen as 4

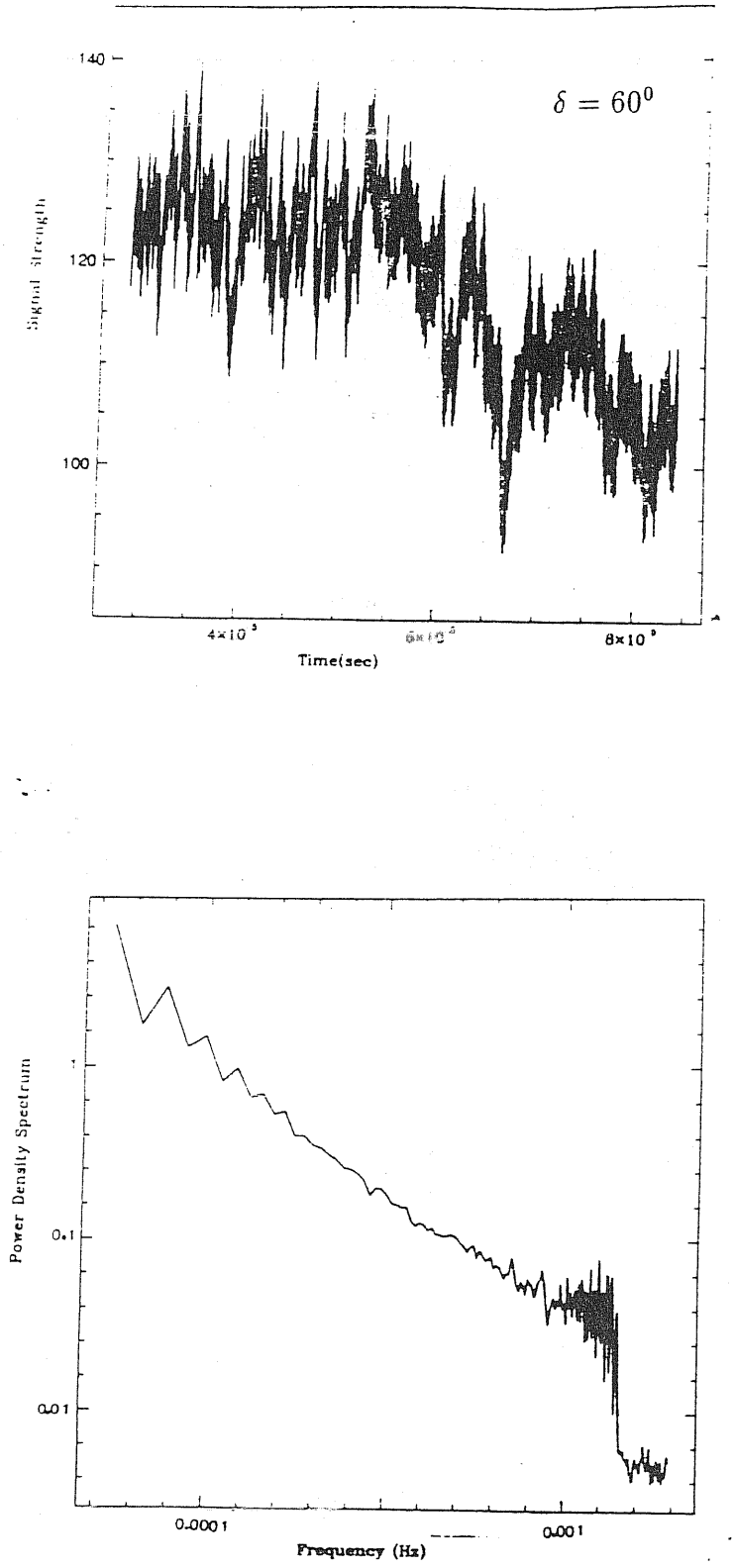

Figure 17. The simulated light curves and their power spectra for viewing angles $\delta = 0^0, 20^0, 40^0, 60^0$ respectively.

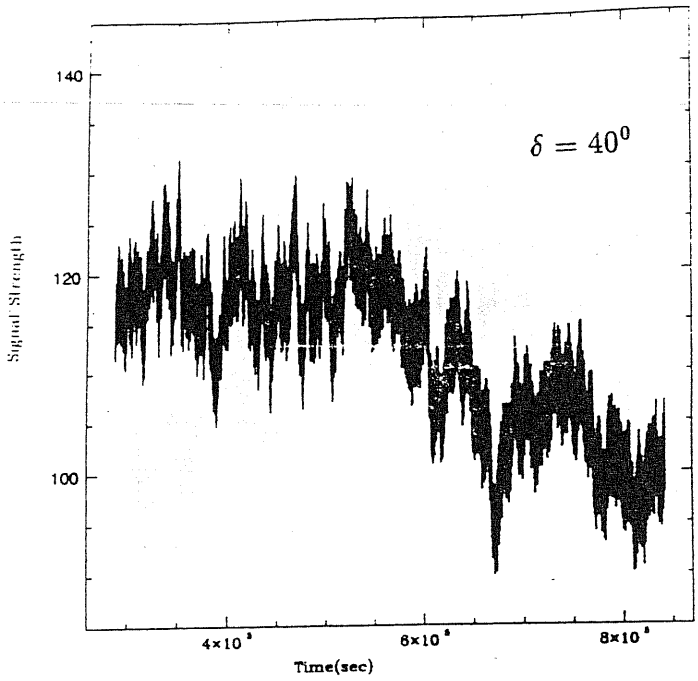
140
120
100
Signal Strength
$\delta = 40^0$
4×10
6×10
8×10
Time(sec)

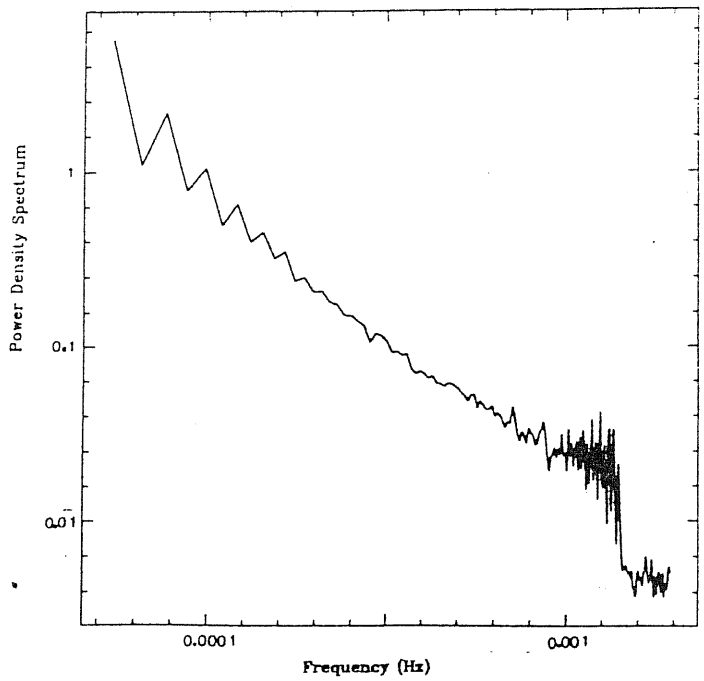
Power Density Spectrum
1
0.1
0.01
0.0001
0.001
Frequency (Hz)

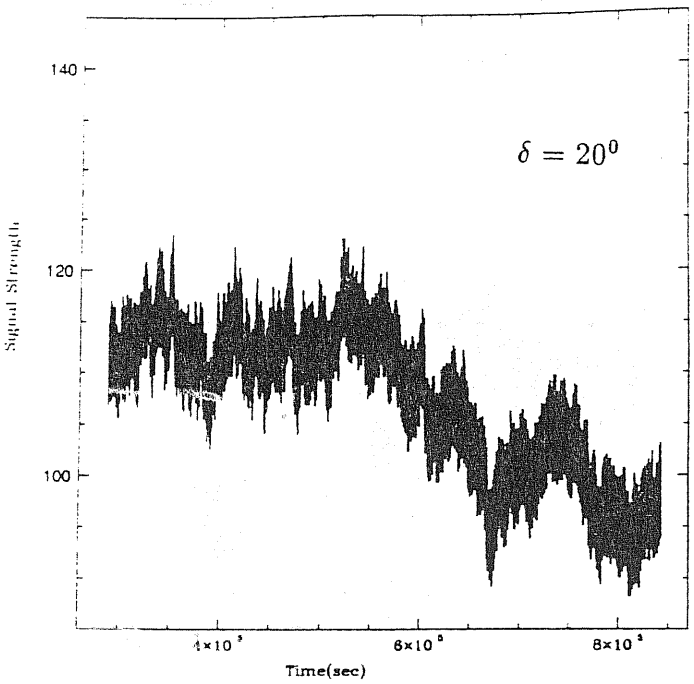
140
120
100
Signal Strength
$\delta = 20^0$
Time(sec)

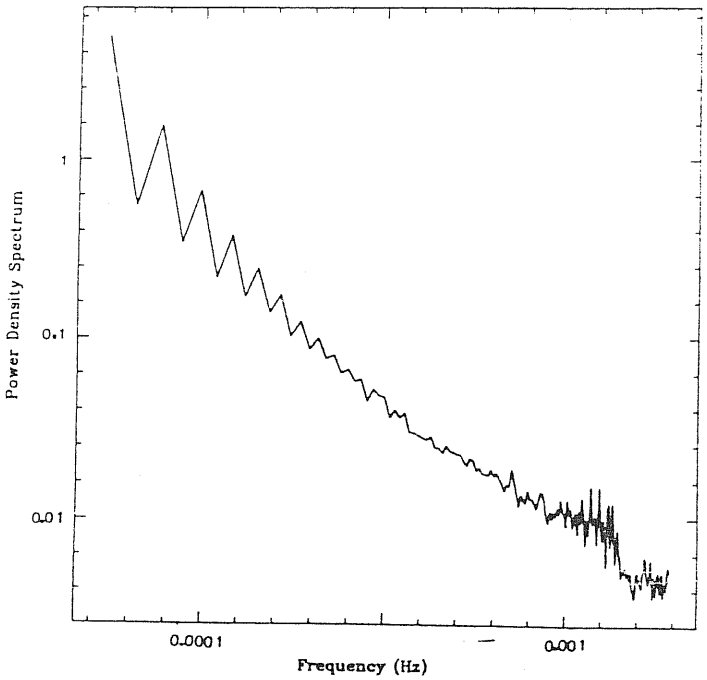
1
0.1
0.01
Power Density Spectrum
0.0001
0.001
Frequency (Hz)

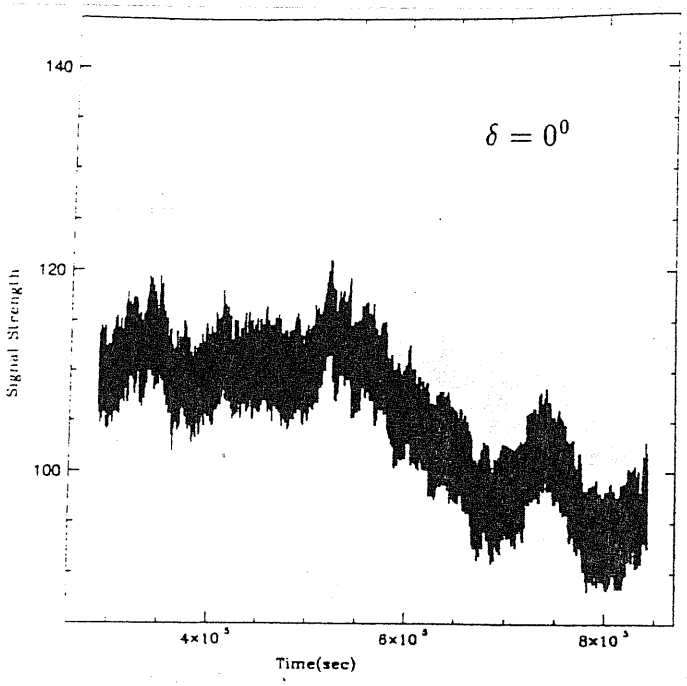
140
120
100
$\delta = 0^0$
Signal Strength
4×10^3
6×10^3
8×10^3
Time(sec)

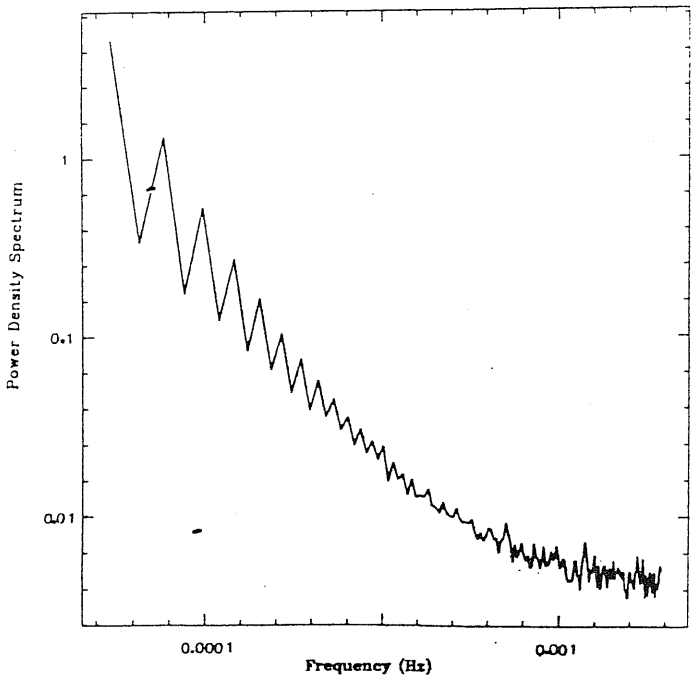
1
0.1
0.01
Power Density Spectrum
0.0001
0.001
Frequency (Hz)

times the orbital period of the outermost orbit. All spots are distributed evenly on the surface of the disk, with the same brightness and the same size. In Fig. 17a the disk is viewed face-on and no variability can be seen apart from the switching on and off of the spots and that of the noise. In Figs. 17b, c, d, as the inclination angle δ increases gradually, the effect of rotation gradually shows up: part of power spectrum due to spots increases above the noise level and its shape changes till it reaches the power-law form predicted by (3.47), $P(\omega) \sim \omega^{-1.7}$. Note that, once above the noise level and dominating the intrinsic part, the slope of the power spectrum due to rotation is completely determined by the disk rotation and the statistics property of the spot, while the inclination angle mostly controls the amplitude.

In Fig. 18, we use an $n(r)$ with the decrease in the surface number density beyond $r = 30M$ in order to model the tendency of disk to be smoother at larger radii. All other parameters are the same as in Fig. 17. Shown in Fig. 18 is power spectrum for the inclination angle $\delta = 60°$. When there is a drop of spot density beyond certain radius, the power spectrum could be flattened below the corresponding orbital frequency.

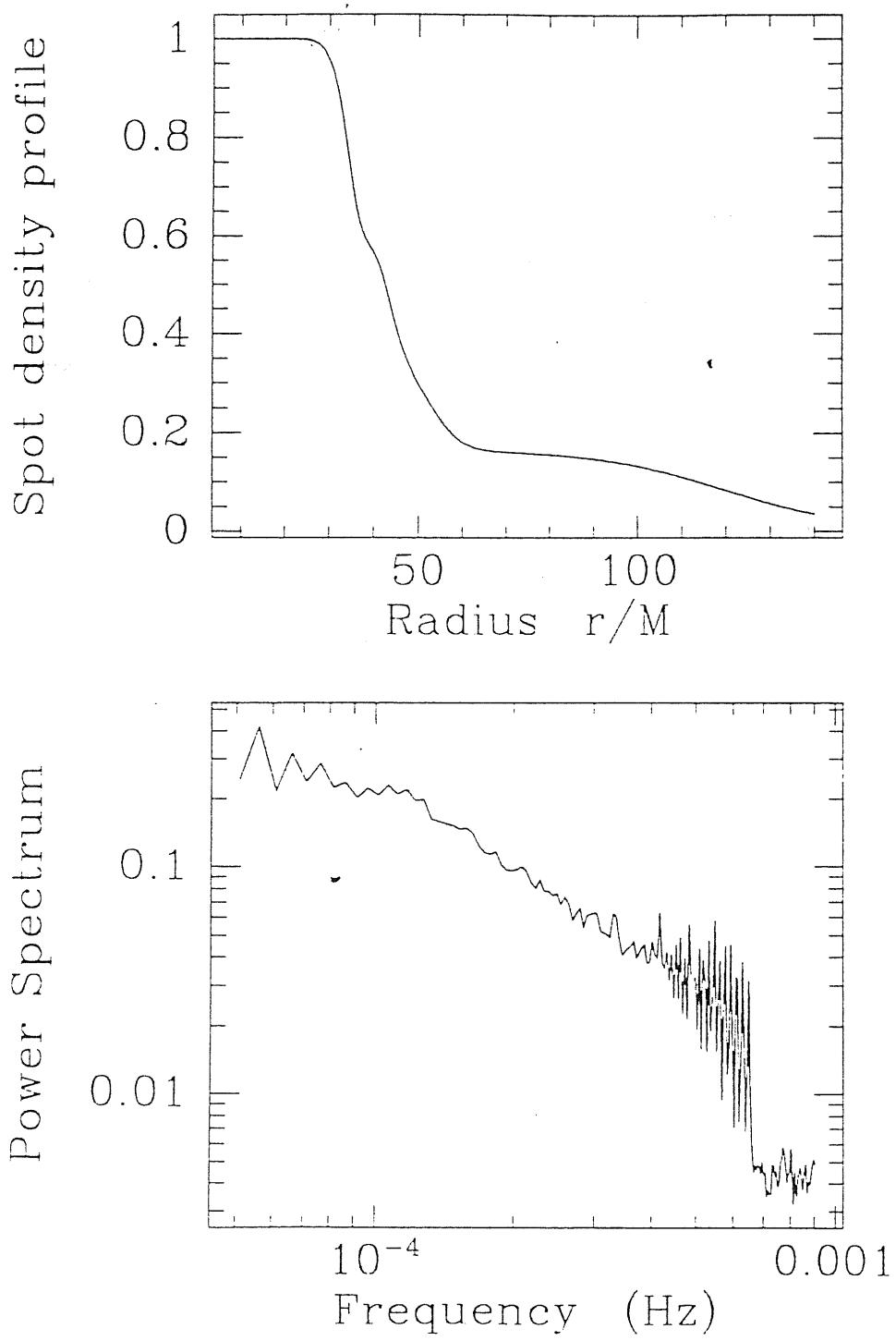

Figure 18. The power spectrum for a decrease surface density profile.

Chapter 4

Conclusions and discussions

So far, we have given a basic description of "hot spot" model and have obtained the result as expected.

The rotation effect does introduce rapid variability in light curve and affect power spectrum in frequency range of $10^{-5} \sim 10^{-3}$ Hz which are connected with orbital frequency of spots.

The statistics of spots plays a very important role in our model. The number density per unit radius $n(r)$, the life time of spots $\tau_s(r)$, the brightness $I(r)$ and the size of spots $\Delta D(r)$ plus its rotation law $\Omega(r)$ totally control the shape of power spectrum. When spots distribute on the surface of disk in a narrow range of r, the power spectrum shows many peaks corresponding to orbital frequency $\Omega(r)$ and its harmonics. When spots spread on a broad range its power spectrum exhibits a power law form $P(\omega) \sim \omega^{-\beta}$. This statistics (spots spread in a broad range) might be true for most AGNs. But the statistics of spots is still unknown at moment, it strongly depends on the spots creation mechanism. Only when we know this mechanism very well can we give

complete description of it.

The inclination angle of observer is also an important parameter. Larger viewing angle introduces larger variability amplitude (larger rotation effect) in intensity. However, this does not mean those sources with larger variability amplitude definitely have a larger inclination angle, because there exist many kinds of intrinsic variability which also contribute to the total power in the rotation frequency range. The inclination angle should anyway be one of the main important factors. The problem is how to tell the difference between rotation induced variability from other intrinsic ones in a given signal ?

Gravitation should be important when observer has a large viewing angle. The intensity can be greatly amplified when the spot is behind the black hole, opposite to the observer. Our future work will be on a full relativistic case. It will be much more complicated than what we have done here, though.

Finally, since the variability of BL Lac object is thought to be associated with the ejected material from the central part, our result does not apply to that class of objects.

ACKNOWLEDGEMENTS

I wish, first of all, to express my sincere gratitude to Professor Marek A. Abramowicz for bringing me to the present field of research and for his constant and enlightening guidance and encouragement throughout the production of the dissertation. I owe a separate debt of thanks to Dr X.H. Zhang and Dr A. Lanza for the discussions in the course of writing. Finally, to all of my tutors and my friends in SISSA who have given me encouragement and assistance, I offer my sincere thanks.

I must assume, however, full responsibility for posssible errors of any sort in the dissertation.

Appendix A

In this appendix, we shall use the definition

$$v_d \equiv v_s \sin\delta$$

for the projected orbital speed of the spot. The light curve of a spot can be represented as

$$u(t) = (1 - v_d \sin\phi_s)^4 E(\phi_s) G(t)$$

where I has been factored out and

$$\phi_s = \Omega_s t + \phi_c + v_d(\cos\phi_c - \cos\phi_s) \quad . \tag{1}$$

In terms of the Fourier transforms of $u(t)$, we can write down the power spectrum density for $u(t)$,

$$\begin{aligned} p(\omega) &= \frac{1}{4\pi}\int_0^{2\pi} d\phi_c \int_{-\infty}^{+\infty} dt \int_{-\infty}^{+\infty} dt' \\ &\quad \times (1 - v_d \sin\phi_s)^4 (1 - v_d \sin\phi_s')^4 E(\phi_s) E(\phi_s') G(t) G(t') e^{-i\omega(t-t')} \end{aligned}$$

Here, we use $E(\phi_s)$ to represent the eclipse,

$$E(\phi_s) = \begin{cases} 1 & |\phi_s - 2n\pi| > \phi_{\text{eclipse}}\,, n = 0, \pm 1, 2, ... \\ 0 & \text{otherwise} \quad ; \end{cases}$$

$G(t)$ is the evolution envelop of the spot intensity; and we assume that the spot has equal chance of being produced at any orbital position ϕ_0.

To compute $p(\omega)$, we first make a Fourier series expansion of $E(\phi_s)$,

$$E(\phi_s) = \sum_n b_n e^{in\phi_s} \quad .$$

We also write, for the compactness purpose,

$$(1 - v_d \sin\phi_s)^4 = \sum_{k=0}^{4} \binom{4}{k} (-v_d)^k \sin^k \phi_s \quad ,$$

$$\sin^k \phi_s = \left(\frac{1}{2i}\right)^k (e^{i\phi_s} - e^{-i\phi_s})^k \quad = \quad \frac{e^{ik\phi_s}}{(2i)^k} \sum_{j=0}^{k} \binom{k}{j} (-1)^j e^{-i2j\phi_s}$$

Then we solve (1) by the iteration method

$$\phi_s^{(0)} = \Omega_s t + \phi_c \quad ,$$

$$\phi_s^{(1)} = \phi_s^{(0)} + v_d(\cos\phi_c - \cos\phi_s^{(0)}) \quad ,$$

$$\phi_s^{(2)} = \phi_s^{(0)} + v_d(\cos\phi_c - \cos\phi_s^{(1)}) \quad ,$$

$$\ldots$$

but stop at the first step. The error of this truncation for $u(t)$ is

$$\begin{aligned}
\frac{\Delta u}{u} &= \frac{4v_d|\sin\phi_s - \sin\phi_s^{(1)}|}{|1 - v_d\sin\phi_s|} \\
&= \frac{8v_d|\cos\frac{\phi_s+\phi_s^{(1)}}{2}\sin(\frac{v_d(\cos\phi_s-\cos\phi_s^{(1)})}{2})|}{|1 - v_d\sin\phi_s|} \\
&= \frac{8v_d|\cos\frac{\phi_s+\phi_s^{(1)}}{2}\sin\left(v_d\sin\frac{\phi_s+\phi_s^{(1)}}{2}\sin\left(\frac{v_d(\cos\phi_s-\cos\phi_s^{(1)})}{2}\right)\right)|}{|1 - v_d\sin\phi_s|} \\
&= \ldots
\end{aligned}$$

It is clear that the error approaches zero faster than any power of v_d for small v_d. For $\phi_s \approx \phi_s^{(1)}$, we make a further expansion,

$$e^{-i(n+k-2j)v_d\cos(\Omega_s t+\phi_c)} = \sum_{p=0}^{\infty}\sum_{s=0}^{p} \frac{1}{(2p)!!}\binom{p}{s}[-i(n+k-2j)v_d]^p e^{i(p-2s)(\Omega_s t+\phi_c)}$$

Similar expansions are made for $(1 - v_d \sin\phi_s')^4$ and $E(\phi_s')$ with the following changes in indices,

$$n \to n' \ , \quad k \to m \ , \quad l \to j \ , \quad p \to q \ , \quad r \to s \ .$$

Of the three integrals in $p(\omega)$, we first integrate over ϕ_c with the aid of the integral representation of the n^{th} order Bessele function

$$J_n(x) = \frac{1}{2\pi i^n} \int_0^{2\pi} e^{ix\cos\psi - in\psi} d\psi$$

and the final result is

$$\begin{aligned} P(\omega) &= \frac{1}{2} \int \frac{I^2(r)}{\tau(r)} n(r) p(\omega; r) dr \\ &= \frac{1}{2} \int \frac{I^2(r)}{\tau(r)} n(r) dr \sum \alpha_N(v_d)^M J_N(K v_d) G_{\omega - N_1\Omega_s} G^{\star}_{\omega + N_2\Omega_s} \end{aligned}$$

Here one is to expand the abbreviations $\sum$, α_N, N, M, K, N_1, N_2 as

$$\sum \to \sum_{\substack{k=0 \\ m=0}}^{4} \sum_{j=0}^{k} \sum_{l=0}^{m} \sum_{\substack{n=-\infty \\ n'=-\infty}}^{\infty} \sum_{\substack{p=0 \\ q=0}}^{\infty} \sum_{s=0}^{p} \sum_{r=0}^{q} \tag{2}$$

$$\alpha_N \ \to \ \binom{4}{k}\binom{k}{j}\binom{4}{m}\binom{m}{l}\binom{p}{s}\binom{q}{r} b_n b_{n'} \frac{(n+k-2j)^p (n'+m-2l)^q (-1)^{p+q+s+r}}{2^{k+m+p+q}\, p!\, q!\, i^{n+n'}}$$

$$N_1 \equiv 2j - k - p + 2s - n \ , \quad N_2 \equiv 2l - m - q + 2r - n' \ , \quad N = N_1 + N_2 \ ,$$

$$K \equiv k + m + n + n' - 2(j + l) \ , \quad M \equiv k + m + p + q \ .$$

Correct to order v_d^3, then

$$\begin{aligned} p(\omega) &= 3(3 + 4v_d^2) \frac{\sin^2 \frac{\omega\tau}{2}}{(\omega)^2} \\ &\quad + 4v_d^2 \Big[\frac{\sin^2 \frac{(\omega - \Omega_s)\tau}{2}}{(\omega - \Omega_s)^2} + \frac{\sin^2 \frac{(\omega + \Omega_s)\tau}{2}}{(\omega + \Omega_s)^2} \\ &\quad - \left(\cos\frac{\Omega_s\tau}{2}\right) \frac{\sin\frac{\omega\tau}{2} \sin\frac{(\omega - \Omega_s)\tau}{2}}{\omega(\omega - \Omega_s)} - \left(\cos\frac{\Omega_s\tau}{2}\right) \frac{\sin\frac{\omega\tau}{2} \sin\frac{(\omega + \Omega_s)\tau}{2}}{\omega(\omega + \Omega_s)} \Big] \\ &\quad + O(v_d^4) \quad . \end{aligned}$$

Bibliography

[1] Abramowicz M. A., Bao G., Lanza A., Zhang X-h.:1989 in *Proceedings of the 23rd ESLAB symposium*, eds. Hunt J. and Battrick, B. (ESA Publication Division, ESTEC, Noordwijk, The Netherlands),

[2] Abramowicz M. A., Bao G., Lanza A., Zhang X-h.:1990 *Ap. J. lett.*, submitted,

[3] Abramowicz M. A., Szuszkiewicz E. :1989 in *Big Bang, Active Galactic Nuclei and Supernovae*, eds. Hayakawa S. and Sato K. (Universal Academic Press, Tokyo),

[4] Alloin D. et al. :1986, *Ap. J.*, **308**, 23,

[5] Asaoka I. :1989, *Publ. Astron. Soc. Japan*, **41**, 736,

[6] Barr P., Clavel J., Giommi P., Mushotzky R., F., Madejski G.: 1986 in *Variability of Galactic and Extragalactic X-ray Sources*, ed. Treves A. (Milano),

[7] Blandford R. D. :1985 in *Active Galactic Nuclei*, ed. Dyson J. E (Manchester University Press),

[8] Burbidge G. R., Burbidge E. M., Sandage A. :1963 *Rev. Mod. Phys.* **35**, 947,

[9] Cavallo G. and Rees M. J. :1978, *Mon. Not. R. Astr. Soc.* **183**, 359,

[10] Cunninghan C. T., Bardeen J. M. :1973, *Ap. J.*, **183**, 237,

[11] Hawley J. : 1987, *Mon. Not. R. Astr. Soc.*, **225**,677,

[12] Lawrence A., Pounds K. A., Watson M. G. and Elvis M. S. :1985,*Mon. Not. R. astr. Soc.* **217**, 685,

[13] Lawrence A., Watson M. G., Pounds K. A., and Elvis M. :1987, *Nature*, **325**, 694,

[14] Makishima K. :1988 in *Physics of Neutron Stars and Black Holes*, ed. Tanaka Y. (Universal Academic Press, Tokyo),

[15] Marshall N., Warwick R. S., Pounds K. A.: 1981 *Mon. Not. R. Astr. Soc.*, **194**,987,

[16] McHardy I. M. :1985, *Space Science Reviews*, **40**, 559,

[17] McHardy I. M. and Czerny B. :1987, *Nature*, **325**, 696,

[18] Misner C. W., Thorne K. S., and Wheeler J. A. :1973, *Gravitation* (W. H. Freeman, San Francisco),

[19] Mittaz J. P. D., Branduardi-Raymont G. :1989, *Mon. Not. R. Astr. Soc.*, **238**, 1029,

[20] Nonan P. L., Gruber J. L., Matteson J. L., Peterson L. E., Rothschild R. E., Doty J. P., Levine A. M., Lewin H. G. and Primini F. A. :1981, *Ap. J.*, **246**, 494,

[21] Perola G. C. et al: 1986, *Ap. J.*, **306**, 508,

[22] Pounds K. A., Nandra K., Stewart G. C., Leighly K. :1989,*Mon. Not. R. Astr. Soc.* **240**, 769,

[23] Pounds K. A., McHardy I. M.:1988 in *Physics of Neutron Stars and Black Holes*, ed. Tanaka Y.

[24] Pounds K. A. and Turner T, J. : 1986 in *Variability of Galactic and Extragalactic X-ray Sources*, ed. Treves A. (Milano),

[25] Rice S. O. :1954, in *Noise and Stochastic Processes*, ed. Wax N., (Dover, London)

[26] Roberto G. A., McHardy I. M. :1989 in *Proceedings of the 23rd ESLAB Symposium*, eds. Hunt J. and Battrick, B. (ESA Publication Division, ESTEC, Noordwijk, The Netherlands),

[27] Robinson I., Schild, A., Schucking, E., eds: 1964 in *Proceedings of Tex Conf. Relative Astrophys., 1st.* (Chicago Univ. Chicago Press),

[28] Syunyaev R. A. :1973, *Soviet Astronomy-AJ*, **6**, 941,

[29] Shakura N. I. and Syunyaev N. I. :1976, *Mon. Not. R. Astr. Soc.* **175** 613,

[30] Tennant A., Mushotzky R. F., Mushotzky R. F., Boldt E., Swank J. :1981, *Ap. J.*, **264**, 92,

[31] Wilson A. S., Ward M. J., Ayon D. J.,Elvis M., Meurs E. J. A. : 1979, *Mon. Not. R. Astr. Soc.*, **187**, 109,

[32] Zhang X-H., Bao G. :1990, *Astron. Astrophys*, (in press).